Article:
Fan, R. orcid.org/0000-0003-1032-4546, Satilmis, H., Vandewalle, N. et al. (16 more authors) (2023) Tasquinimod suppresses tumor cell growth and bone resorption by targeting immunosuppressive myeloid cells and inhibiting c-MYC expression in multiple myeloma. Journal for ImmunoTherapy of Cancer, 11 (1). e005319. ISSN 2051-1426

https://doi.org/10.1136/jitc-2022-005319

Journal for ImmunoTherapy of Cancer

Tasquinimod suppresses tumor cell growth and bone resorption by targeting immunosuppressive myeloid cells and inhibiting c-MYC expression in multiple myeloma

Rong Fan ,[1] Hatice Satilmis,[1] Niels Vandewalle,[1] Emma Verheye,[1,2,3] Philip Vlummens,[1,4] Anke Maes,[1] Catharina Muylaert,[1] Elke De Bruyne,[1] Eline Menu,[1] Holly Evans,[5] Andrew Chantry,[5] Nathan De Beule ,[6] Dirk Hose,[1] Marie Törngren,[7] Helena Eriksson,[7] Karin Vanderkerken,[1] Ken Maes ,[8] Karine Breckpot,[9] Kim De Veirman [1]

To cite: Fan R, Satilmis H, Vandewalle N, *et al*. Tasquinimod suppresses tumor cell growth and bone resorption by targeting immunosuppressive myeloid cells and inhibiting c-MYC expression in multiple myeloma. *Journal for ImmunoTherapy of Cancer* 2023;**11**:e005319. doi:10.1136/jitc-2022-005319

► Additional supplemental material is published online only. To view, please visit the journal online (http://dx.doi.org/10.1136/jitc-2022-005319).

Accepted 30 December 2022

For numbered affiliations see end of article.

Correspondence to
Professor Kim De Veirman; kim.de.veirman@vub.be

ABSTRACT

Background Immunotherapy emerged as a promising treatment option for multiple myeloma (MM) patients. However, therapeutic efficacy can be hampered by the presence of an immunosuppressive bone marrow microenvironment including myeloid cells. S100A9 was previously identified as a key regulator of myeloid cell accumulation and suppressive activity. Tasquinimod, a small molecule inhibitor of S100A9, is currently in a phase Ib/IIa clinical trial in MM patients (NCT04405167). We aimed to gain more insights into its mechanisms of action both on the myeloma cells and the immune microenvironment.

Methods We analyzed the effects of tasquinimod on MM cell viability, cell proliferation and downstream signaling pathways in vitro using RNA sequencing, real-time PCR, western blot analysis and multiparameter flow cytometry. Myeloid cells and T cells were cocultured at different ratios to assess tasquinimod-mediated immunomodulatory effects. The in vivo impact on immune cells (myeloid cell subsets, macrophages, dendritic cells), tumor load, survival and bone disease were elucidated using immunocompetent 5TMM models.

Results Tasquinimod treatment significantly decreased myeloma cell proliferation and colony formation in vitro, associated with an inhibition of c-MYC and increased p27 expression. Tasquinimod-mediated targeting of the myeloid cell population resulted in increased T cell proliferation and functionality in vitro. Notably, short-term tasquinimod therapy of 5TMM mice significantly increased the total $CD11b^+$ cells and shifted this population toward a more immunostimulatory state, which resulted in less myeloid-mediated immunosuppression and increased T cell activation ex vivo. Tasquinimod significantly reduced the tumor load and increased the trabecular bone volume, which resulted in prolonged overall survival of MM-bearing mice in vivo.

Conclusion Our study provides novel insights in the dual therapeutic effects of the immunomodulator tasquinimod and fosters its evaluation in combination therapy trials for MM patients.

WHAT IS ALREADY KNOWN ON THIS TOPIC

⇒ Tasquinimod is a new immunomodulatory treatment for multiple myeloma (MM) that is in phase I/II clinical evaluation in patients with relapsed/refractory MM.

WHAT THIS STUDY ADDS

⇒ Our study provides novel insights in the dual therapeutic effects of the immunomodulator tasquinimod, targeting both the tumor cells and its suppressive microenvironment to hamper MM progression.

HOW THIS STUDY MIGHT AFFECT RESEARCH, PRACTICE OR POLICY

⇒ This study elucidates the mechanism of action of tasquinimod and fosters its evaluation in combination therapy trials for MM patients.

INTRODUCTION

Multiple myeloma (MM) is a rare B cell malignancy, characterized by the uncontrolled growth of malignant plasma cells in the bone marrow.[1] The complex crosstalk between plasma cells and immune cell populations makes the MM bone marrow niche an immunosuppressive environment favoring MM cell growth, survival, and drug resistance.[2–4] Several immunotherapeutic approaches including monoclonal antibodies, antibody-drug conjugates, bispecific antibodies, and chimeric antigen receptor T cell therapy emerged as promising therapies for MM patients.[5 6] However, efficacy and long-term anti-MM T cell responses are suggested to be hampered by the presence of a strong immunosuppressive environment.[7 8]

Tasquinimod is a small-molecule oral inhibitor and a second-generation quinoline-3-carboxamide compound.[9] Tasquinimod binds the inflammatory protein S100A9 and inhibits its interaction with the proinflammatory toll-like receptor 4 (TLR4) and receptor of advanced glycation end products (RAGE).[10 11] Besides its high affinity for S100A9, binding of tasquinimod to histone deacetylase 4 (HDAC4) and modulation of the thrombospondin-1 protein has been demonstrated as well.[12 13] Originally tested for the treatment of prostate cancer, tasquinimod exerts immunomodulatory, antiangiogenic and antimetastatic effects in various preclinical cancer models.[13 14] While S100A9 expression is low/absent on MM cells, previous work by our group demonstrated the abundant expression of S100A9 by myeloid-derived suppressor cells (MDSCs) in the bone marrow niche and identified this cell population as a key regulator of MM progression.[15] A better understanding of the direct and indirect anticancer effects of tasquinimod is critical to predict its clinical impact and propose new combination therapies for MM patients.

In this study, we evaluated the effect of tasquinimod on MM cells, myeloid cells (including MDSCs, macrophages, and dendritic cells (DCs)) and T cell activation using in vitro co-culture assays and in vivo short-term treatment of myeloma-bearing mice. We aimed to provide more mechanistic insights into the observed tasquinimod-mediated antitumor effects. Effects on tumor growth, bone disease and survival were further evaluated in immunocompetent MM models.

MATERIAL AND METHODS

Animals

C57BL/KaLwRij mice were purchased from Envigo (Horst, The Netherlands).

Cell culture

Three human MM cell lines (LP-1, OPM-2, RPMI-8226) and murine myeloma cell lines (5TGM1, 5TGM1-eGFP, 5T33MMvt) were cultured in RPMI-1640 medium (Gibco; Thermo Fisher Scientific, Waltham, Massachusetts, USA) supplemented with 10% fetal bovine serum (FBS) (Biochrom AG, Berlin, Germany), 100 U/mL penicillin, 100 µg/mL streptomycin and 2 mM L-glutamine (Lonza, Basel, Switzerland). The human stromal cell line HS-5 was cultured in DMEM medium supplemented with 10% FBS, 1% sodium pyruvate, 1% MEM NEAA (Thermo Fisher Scientific), 100 U/mL penicillin, 100 µg/mL streptomycin and 2 mM L-glutamine. The human MM cell lines LP-1, OPM-2, RPMI-8226 and HS-5 cells were obtained from ATCC (Molsheim, France) and identity of the cell lines was yearly validated by short-tandem repeat analysis. Cell lines were regularly tested for mycoplasma contamination and passaged no more than 1 month prior to experiments (#LT07-418, Lonza, USA).

Compounds

For in vitro experiments, tasquinimod was purchased from Sigma-Aldrich (Diegem, Belgium) and dissolved in dimethylsulfoxide at a stock concentration of 5 mM. For the final concentration, we chose the concentrations 10 µM and 25 µM. For in vivo experiments, tasquinimod was kindly provided by Active Biotech AB (Lund, Sweden) and was administered orally via the drinking water at a dose of 30 mg/kg.

Cell proliferation and apoptosis assay

MM cell lines were cultured at a concentration of 5.0×10^5 cells/mL and HS-5 cells were seeded at a concentration of 1.0×10^5 cells/mL. Cells were treated with increasing concentrations of tasquinimod (10, 25 µM) for 24 hours, 48 hours, 72 hours and 120 hours. A 1 mg/mL bromodeoxyuridine (BrdU) (#B5002, Sigma) was added 4 hours before sample collection. Samples were washed with FACS flow and stained for 10 min with paraformaldehyde at 4°C. The cells were incubated overnight in PBS (Gibco) 0.2% Tween (Sigma-Aldrich) at room temperature, washed twice with FACS flow, stained for 30 min with 2 M HCl and washed with both FACS flow and a mixture of PBS+0.5% Triton X (Sigma-Aldrich)+10% FBS. Cells were then stained with 3 µL of anti-BrdU-Fluorescein (#112022693011, Sigma-Aldrich) in 50 µL of PBS+0.5% Triton X+10% FBS and incubated in the dark for 30 min. After a washing step, the percentage of $BrdU^+$ cells was detected by flow cytometry using the FACS Canto flow cytometer (BD Biosciences, Belgium). Apoptosis was measured by flow cytometry using Annexin-V and 7-aminoactinomycin D staining (BD Biosciences, Erembodegem, Belgium).

Colony-forming unit assay

Clonogenic potential of human MM cell lines was assessed through colony growth in MethoCult media (H4230, M3231, STEMCELL Technologies, Canada) in the presence of dimethylsulfoxide (control) or tasquinimod. Briefly, LP-1 and 5TGM1 cells (2000 cells/well) were treated with different concentrations of tasquinimod (10, 25 µM). Each plate contained RPMI-1640 media consisting of Methylcellulose-Based Media, 10% FBS, 100 U/mL penicillin and 100 µg/mL streptomycin. Plates were incubated at 37°C, 5% CO_2 for 14 days. The colonies were photographed using the EVOS M7000 Imaging System (Thermo Fisher Scientific).

RNA sequencing and analysis

LP-1 cells were cultured for 6 hours and 24 hours with or without 25 µM of tasquinimod. Total RNA was extracted and purified using the NucleoSpin RNA plus kit (Macherey-Nagel, Düren, Germany). Sample quality was checked by calculating the RNA integrity number (RIN value) using fragment analyser (Agilent). The RNA sequencing (RNA-seq) library preparation was performed with 150 ng RNA using the Illumina KAPA RNA HyperPrep kit with RiboErase (HMR) (Illumina, Cambridge, UK). Paired-end RNA-seq (2*100 bp) was done with an Illumina NovaSeq 6000 seqencing instrument (Illumina, Cambridge, UK) and read pairs were

mapped to the human GRCh37 reference genome using the STAR alignment algorithm.[16] All statistical analyses were performed with the statistics software R (V.4.1.2) and R packages obtained though the BioConductor project (https://www.bioconductor.org).[17] The expression level of each gene was summarized and normalized using DESeq2 R/Bioconductor package and differential expression analysis was performed using DESeq2 pipeline.[18] P values were adjusted to control the global false discovery rate (FDR) across all comparisons with the default option of the DESeq2 package. Genes were considered differentially expressed if they had an adjusted p value equal or lower than 0.05 and a fold change of more or equal to 2. Pathway enrichment analyses were performed using online curated gene set collection on the Gene Set Enrichment Analysis software (GSEA) (Broad Institute, UC San Diego). GSEA was performed to determine differentially expressed genes that were enriched in gene lists extracted from human MSigDB database V.2022.1 to determine enrichment in gene sets from the hallmark gene sets. Raw data files are available in the public data repository 'ArrayExpress' (Accession number: E-MTAB-11787).

Western blot

MM cells were cultured at a density of 5.0×10^5/mL and were treated with tasquinimod for 6 hours and 24 hours. Cells were lysed in cell lysis buffer including protease (Roche) and phosphatase inhibitors (Sigma). Western blot analysis on these cell lysates was performed as previously described.[19] The following primary antibodies were used: mouse-anti p-STAT3 (Y705) (#9145), p-STAT3 (S727) (#9138), rabbit-anti STAT3 (#4094), c-MYC (#5605), p27 Kip1(#3688), HDAC4 (#2072), α-TUBULIN (#2144), β-ACTIN (#4907) and horseradish peroxidase (HRP)-coupled anti-rabbit (#7074) and anti-mouse (#7076) secondary antibodies; all purchased from Cell Signaling Technology (Boston, Massachusetts, USA). The bands were visualized and captured using Pierce ECL Western Blot Substrate (Thermo Scientific) and Li-Cor Odyssey Fc (Bad Homburg, Germany). Pixel densities were quantified using Image J.

RNA isolation and real-time PCR

The total RNA was isolated by RNeasy mini kit (QIAGEN, Hilden, Germany) and converted to cDNA by the Verso cDNA Synthesis Kit (Thermo Fisher Scientific, Waltham, Massachusetts, USA). Expression level of mRNA was quantified by Real-time PCR with PowerUp SYBR Green Master Mix (Thermo Fisher Scientific) using the ABI 7900TH Real-time PCR System (Applied Biosystems). ABL was included as an internal control. Relative mRNA expression normalized to ABL was carried out using the $2^{-\Delta\Delta Ct}$ method. Gene specific primers were purchased at Integrated DNA Technologies (Leuven, Belgium). Primer sequences are listed in online supplemental table S1.

Magnetic activated cell sorting of bone marrow derived CD11b$^+$ cells

Bone marrow was flushed from the femurs, tibiae and humeri of naïve and diseased mice; followed by red blood cell lysis. CD11b$^+$ cells were isolated by magnetic activated cell sorting using human/mouse CD11b MACS Beads (Miltenyi Biotec, Bergisch Gladbach, Germany) according to the manufacturer's instructions.

Flow cytometry analysis

The antibodies used for all experiments included CD11b-APCCy7 (#101226), Ly6G-PECy7 (#127618), CD3-APCCy7 (#100330), F4/80-APC (#123116), CD206-PE (#141706), MHCII-PE (#107647), MHCII-PECy7 (#107629), CD11c-APC (#117309), CD86-PECy7 (#105014) from Biolegend (Biolegend, San Diego, California, USA) and Ly6C-APC (#560595) from BD (BD Biosciences, UK). BD FACSDiva Software (Becton Dickinson) was used to acquire data. Analysis of data involved postacquisition gating using FlowJo software (Tree Star: Ashland, Oregon, USA).

T cell proliferation assay

To assess T cell proliferation in vitro, spleens were isolated from naïve C57BL/KaLwRij mice, followed by red blood cell lysis. Mononuclear cells (2.0×10^6/mL) were stained by carboxyfluorescein succinimidyl ester (CFSE) (0.1 µM/L) (Invitrogen, Carlsbad, California, USA) for 10–15 min at 37°C, centrifuged and resuspended in RPMI-1640 supplemented with 10% FBS, 10% HEPES (Sigma), 1% sodium pyruvate, 1% MEM NEAA and 20 µM β-ME (Sigma). T cells were cocultured with CD11b$^+$ cells at different ratios and stimulated with 2 µL Dynabeads Mouse T-Activator CD3/CD28 (Invitrogen) and tasquinimod (25 µM) in MM conditioned medium for 72 hours. Conditioned medium was prepared from 5TGM1 cells, cultured for 48 hours in RPMI-1640 medium (with 10% FBS, 100 U/mL penicillin, 100 µg/mL streptomycin and 2 mM L-glutamine) at a density of 1×10^6 cells/mL. T cell proliferation was detected by flow cytometric CFSE dilution after CD3-APCCy7 staining.

For the ex vivo T cell proliferation assay, naïve-derived splenic T cells were cocultured with CD11b$^+$ cells isolated from tasquinimod treated and untreated 5TGM1 MM-bearing mice (n=5). As described previously, T cells were cultured with different ratios CD11b$^+$ cells for 72 hours, in the presence of CD3/CD28 microbeads. After staining by CD3-APCCy7, T cell proliferation assay was performed using flow cytometry.

IFN-γ determination by ELISA

Supernatant was collected from the T cell proliferation assays and was analyzed for IFN-γ secretion by ELISA. Serum collected from the blood of the 5TGM1 model and 5T33MM models was subjected to an IFN-γ ELISA. ELISA was carried out according to the manufacturer's instructions (#88-7314-88, Invitrogen).

In vivo experiments

For in vivo experiments, the sample size was calculated using G*Power. The 5TGM1 model is propagated by intravenous injection of 1.0×10^6 5TGM1-eGFP cells into 6–8 weeks old female C57BL/KaLwRij mice.[20 21] For the 5T33MM mouse model, the 5T33MMvv cell line originated spontaneously in elderly C57BL/KaLwRij mice and have since been propagated in vivo by intravenous transfer of the diseased bone marrow (5.0×10^5 cells/mouse) into young syngeneic mice.[20] The treatment group (n=10/group) received tasquinimod (30 mg/kg in daily drinking water) from day 1 after tumor cell inoculation. When the mice showed signs of disease (eg, hind-limb paralysis), all mice were sacrificed. For short-term exposure (n=5/group), 5TGM1 mice were treated with/without tasquinimod for 10 days.

Tumor load was assessed using flow cytometry (GFP^+ in the bone marrow, 5TGM1 model) or by cytosmear staining with May-Grünwald Giemsa (% plasmacytosis in the bone marrow, 5T33MM model). In addition, M-protein in the blood was determined by means of serum electrophoresis. Immune cell populations were evaluated by flow cytometry. One femur from the 5TGM1 model was dissected and stored in 70% EtOH for micro-CT analysis. Micro-CT was performed on distal femurs of mice with the Skyscan 1172 system (Bruker, Kontich, Belgium) as described previously.[22] To determine the effect of tasquinimod on survival (n=10/group), a similar experiment was performed in the 5TGM1 model. Treatment continued until each animal showed signs of morbidity, namely hind-limb paralysis, at which point they were sacrificed.

Statistical analysis

Results were analyzed with GraphPad Prism V.9 software (GraphPad Software, La Jolla, California, USA). A Mann-Whitney U test and Unpaired t-test was used to compare two groups, One-way analysis of variance was used to compare multiple groups. For the survival study, a Kaplan-Meier analysis and log-rank test was performed. All data represent the mean±SD. *p<0.05; **p<0.01; ***p<0.001, ****p<0.0001 were considered statistically significant.

RESULTS

Tasquinimod directly inhibits the proliferation and c-MYC expression in human MM cell lines

To evaluate the direct antitumor effect of tasquinimod in MM, different human myeloma cell lines (LP-1, OPM-2 and RPMI-8226) and the murine 5TGM1 cell line were incubated with increasing concentrations of tasquinimod for 24 hours, 48 hours, 72 hours and 120 hours. While tasquinimod had no effect on the number of apoptotic MM cells (figure 1A, online supplemental figure S1A,C), a significant decrease could be found in the percentage of proliferating MM cells (figure 1B, online supplemental figure S2). Furthermore, no effect could be observed on the apoptosis and proliferation of stromal HS-5 cells after tasquinimod treatment (figure 1C,D, online supplemental figure S2B). Using a colony-forming unit assay, we demonstrated a significant reduction in the number of colonies after 14 days in the presence of tasquinimod (figure 1E). Altogether, these data indicate that tasquinimod inhibits MM cell growth and proliferation in vitro.

To obtain further mechanistic insights into the tasquinimod-mediated antiproliferative effect of MM cells, we performed RNA sequencing of LP-1 cells, treated with tasquinimod for 6 hours and 24 hours. We found 9 upregulated and 21 downregulated genes after 6 hours of tasquinimod treatment, which increased to 35 upregulated and 47 downregulated genes at 24 hours (online supplemental table S2). Gene Ontology analysis revealed a consistent upregulation of genes involved in migration, metabolism and proliferation (online supplemental figure S3). To further investigate the essential regulatory genes in the antitumor mechanism of tasquinimod, we performed gene set enrichment analysis (GSEA) on RNA-seq data (figure 2A). Interestingly, the gene sets of IL6-JAK-STAT3 and MYC targets were significantly less enriched in the tasquinimod-treated group than in the control group (figure 2B). Using western blot, we confirmed a significant downregulation in p-STAT3 (Y705, S727) and c-MYC levels after tasquinimod treatment in all tested cell lines (figure 2C, online supplemental figure S4). These effects were also associated with increased expression of cyclin dependent kinase inhibitor p27 Kip1, most clearly observed in LP-1 (24 hours), RPMI-8226 (6 hours) and 5TGM1 (6 hours, 24 hours) cells.

As we previously found low to absent expression of S100A9 in MM cells, we analyzed the expression of HDAC4, another molecular target of tasquinimod which was also previously linked to c-MYC expression in primary patient samples and human MM cell lines.[23 24] HDAC4 is expressed in MM cell lines and bone marrow plasma cells, at all stages of disease progression, and correlates with an adverse prognosis in newly diagnosed MM patients (online supplemental figure S5A-C). HDAC4 expression was decreased after tasquinimod treatment in the murine 5TGM1 cells, while it remained stable in the human MM cell lines (figure 2C). This result could be explained by the allosteric binding of tasquinimod to the regulatory Zn^{2+} binding domain of HDAC4 that locks the protein in a conformational state.[12] To evaluate whether the decrease in c-MYC could be associated with the targeting of HDACs, we treated MM cells with a class I/II HDAC inhibitor panobinostat and observed a similar reduction in pSTAT3 and c-MYC expression in MM cell lines (online supplemental figure S5).Taken together, these results indicate that the tasquinimod-mediated HDAC4-c-MYC targeting could be a promising therapeutic approach for MM patients.

Tasquinimod reduces the MDSC suppressive capacity and increases T cell proliferation in vitro

MDSCs are a suppressive population in the MM bone marrow microenvironment and are a major target to re-establish T cell activity, particularly in the context

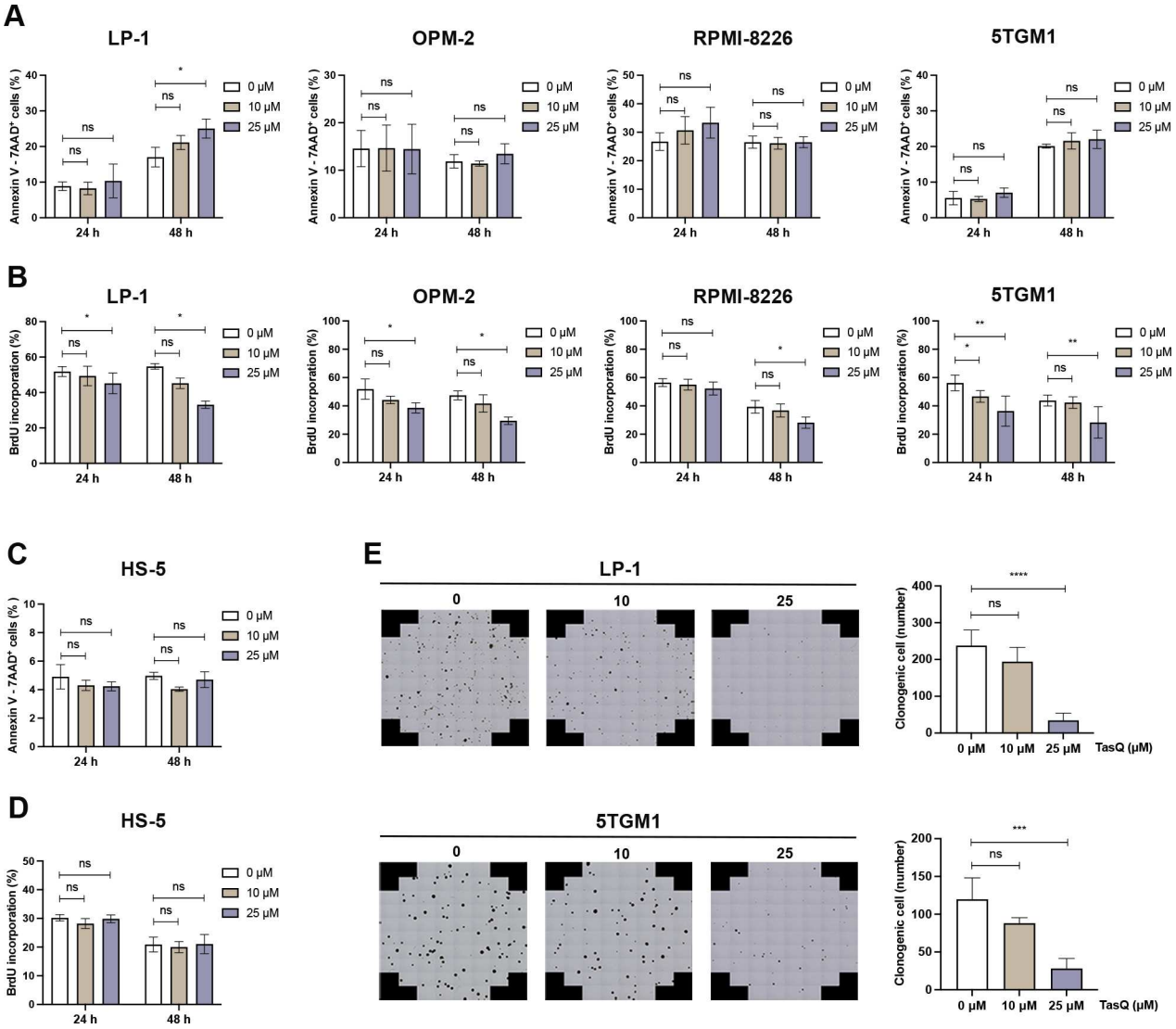

Figure 1 Tasquinimod inhibits MM cell proliferation and reduces colony formation in vitro. (A) Apoptosis was analyzed by flow cytometry using Annexin V/7-AAD staining of tasquinimod-treated MM cell lines including LP-1, OPM-2, RPMI-8226 and 5TGM1 at indicated concentrations for 24 and 48 hours (n=3). (B) Cell proliferation of tasquinimod-treated MM cells (10, 25 μM) was investigated using BrdU staining at 24 hours and 48 hours. Various human MM cell lines were tested including LP-1 (n=3), OPM-2 (n=3), RPMI-8226 (n=4) and 5TGM1 (n=5). (C) Apoptosis and cell proliferation of the human stromal cell line HS-5 treated/untreated with tasquinimod (10, 25 μM) was detected by Annexin V/7-AAD (n=3) and BrdU staining (n=4). (D) Methylcellulose colony formation assays were used for LP-1 and 5TGM1 cell lines treated with vehicle or tasquinimod (10, 25 μM) for 14 days. Quantification of colony numbers was also shown (n=4). *p<0.05, **p<0.01, ***p<0.001, ****p<0.0001, Mann-Whitey U test, Error bars indicate SD. 7-AAD, 7-aminoactinomycin D; MM, multiple myeloma; ns, not significant.

of immunotherapeutic approaches.[25] As we previously demonstrated a high S100A9 expression in MDSCs, we investigated the effect of tasquinimod on MDSC-mediated immune suppression using a T cell proliferation assay.[15] Bone marrow derived myeloid cells ($CD11b^+$) were cocultured with spleen cells at different ratios in MM conditioned medium (derived from 5T33 and 5TGM1 MM cel lines), and T cells were stimulated for 72 hours using anti-CD3/CD28 microbeads. Tasquinimod significantly increased the % $CD3^+$ T cells and T cell proliferation at a 1/2 and 1/4 ratio (MDSCs:T), which was associated with increased IFN-γ secretion (figure 3A,B, online supplemental figure S6A-C). Tasquinimod-treated T cells, without MDSCs, demonstrated a reduced proliferative capacity; indicating that the tasquinimod-mediated effect on T cell activation is solely mediated by targeting the MDSC's suppressive function (figure 3A). Interestingly, we could not observe any direct effect of tasquinimod on the cell viability of MM derived MDSCs (online supplemental figure S7)

As monocytic MDSCs, in contrast to monocytes, are described to differentiate into immunosuppressive macrophages and are associated with elevated S100A8/A9 proteins, we evaluated the effect of tasquinimod on macrophage differentiation markers (figure 3C, online supplemental figure S6D). Twenty-four hours after tasquinimod treatment of MM derived myeloid cells ($CD11b^+$), we observed a significant decrease in the M2 macrophage

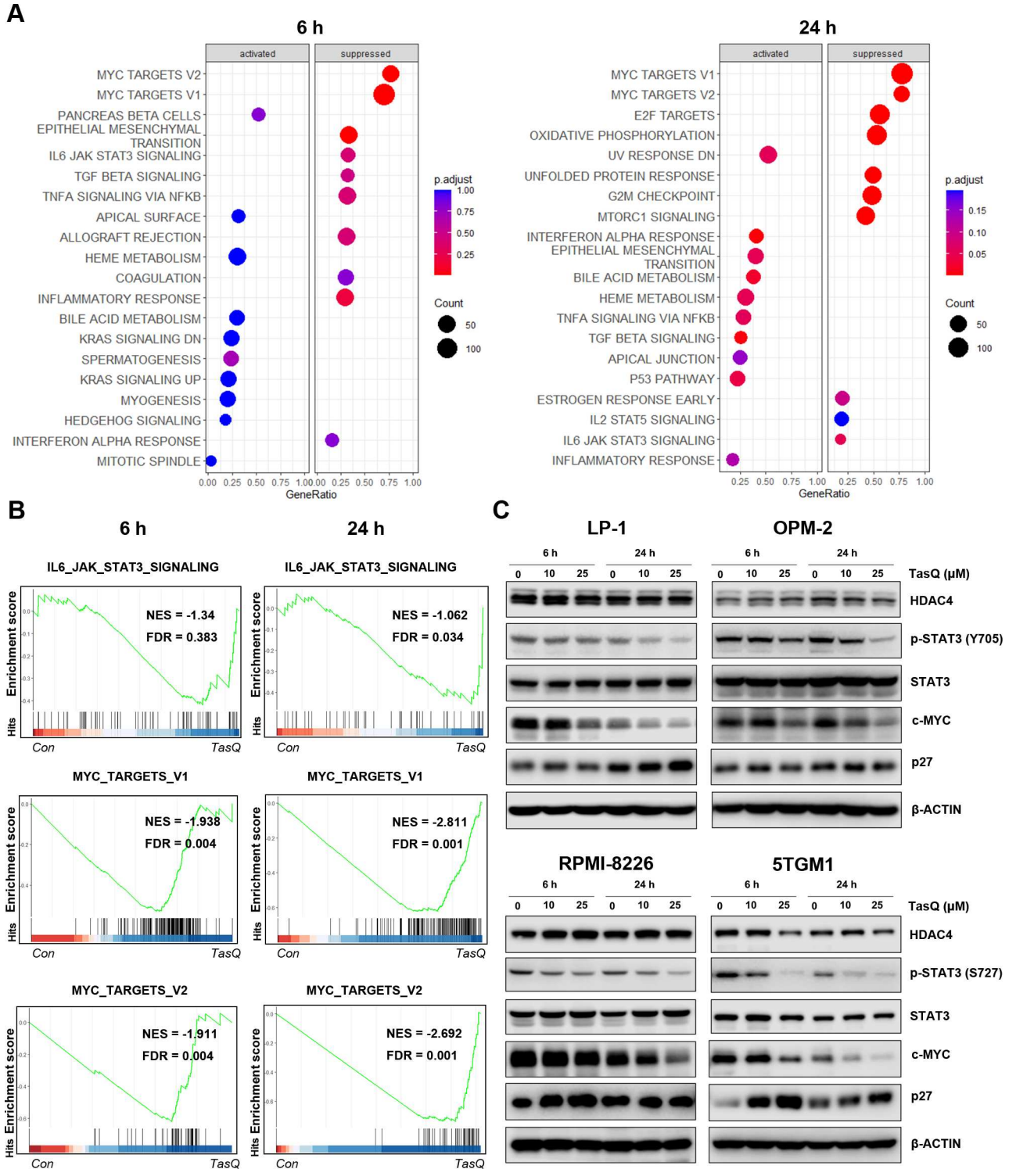

Figure 2 Tasquinimod-mediated downregulation of c-MYC expression in MM cells in vitro. (A) The bubble plot shows the top 20 differentially regulated (activated/suppressed) pathways in the tasquinimod-treated group compared with the control group (6, 24 hours) (n=3). (B) Gene set enrichment analysis (GSEA) of the IL6-JAK-STAT3 and MYC targets V1, V2 gene signature in LP-1 cells after treatment with either 25 μM of tasquinimod or DMSO for 6 hours and 24 hours. GSEA of differentially expressed genes was determined by querying the MSigDB. False discovery rate (FDR) and normalized enrichment scores (NES) are indicated (n=3). (C) LP-1, OPM-2, RPMI-8226 and 5TGM1 cells were cultured with tasquinimod (TasQ) (10, 25 μM) for 6 hours and 24 hours. Whole-cell lysates were subjected to Western blot using HDAC4, anti-Phospho-Stat3 (Tyr705, S727), anti-Stat3, anti-c-MYC, anti-p27 Kip and anti-β-Actin antibodies (n=5). HDAC4, histone deacetylase 4.

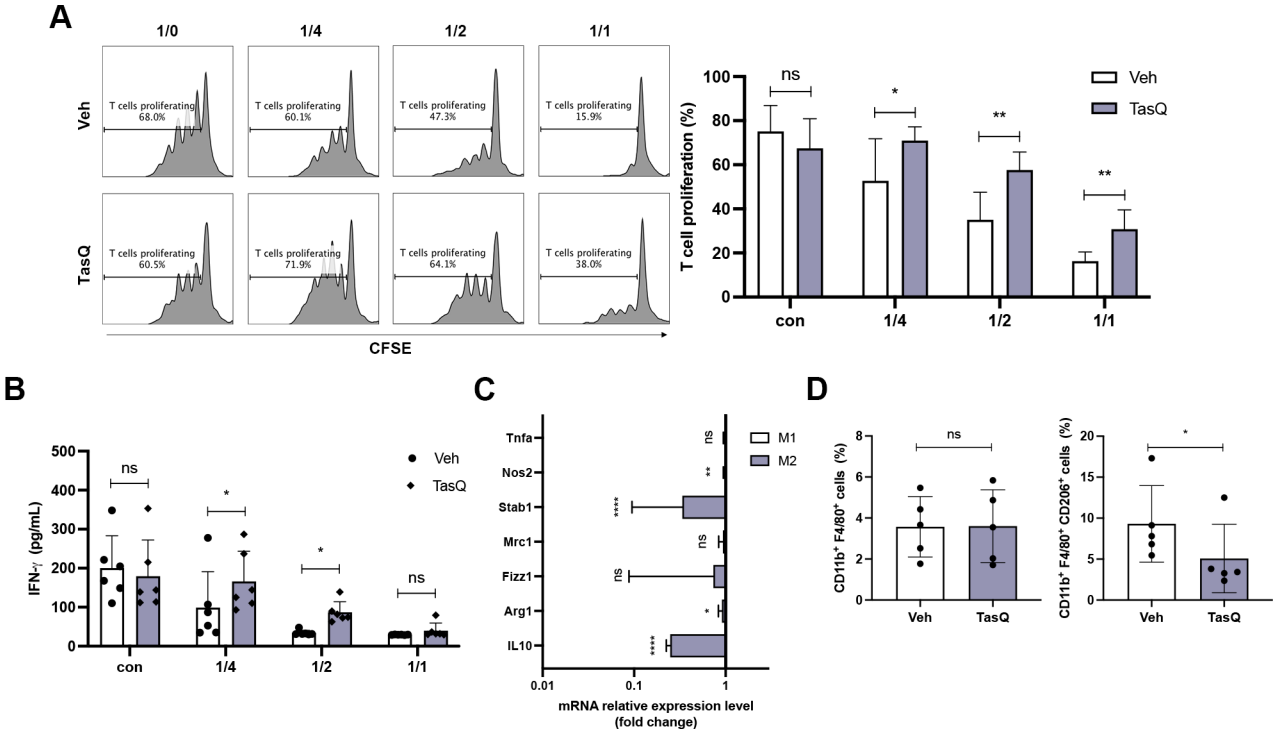

Figure 3 Tasquinimod reduces the MDSC suppressive capacity and increases T cell proliferation in vitro. (A) MACS sorted CD11b$^+$ BM cells were cocultured in the presence of 5TGM1 MM conditioned medium, CD3/CD28 microbeads and splenic CFSE-labeled T cells of naive mice with/without tasquinimod (TasQ). MDSC and T cells were cocultured at a ratio of 1/4, 1/2 and 1/1, respectively. After 72 hours, T cell proliferation was analyzed using flow cytometry (n=8, Mann-Whitey U test). (B) Supernatant was collected from this assay and IFN-γ was analyzed by ELISA (n=8, Mann-Whitey U test). (C) CD11b$^+$ cells were sorted from the BM of the 5TGM1MM model and treated with vehicle or tasquinimod for 24 hours. The mRNA level of genes was measured with RT-qPCR and calculated with the ΔΔC. The data are expressed relative to their respective controls set to 1 (n=5, unpaired t-test). (D) The CD11b$^+$ F4/80$^+$ population and M2 macrophage subset (CD11b$^+$ F4/80$^+$ CD206$^+$) were detected by flow cytometry (n=5, Mann-Whitey U test). *p<0.05, **p<0.01, ****p<0.0001. Error bars indicate SD. BM, bone marrow; CFSE, carboxyfluorescein succinimidyl ester; MACS, magnetic-activated cell sorting; MDSC, myeloid-derived suppressor cell; MM, multiple myeloma.

markers Arginase-1 (Arg1) and Stabilin-1 (Stab1). Stab1 is a scavenger receptor which has been reported to be expressed by tumor-associated macrophages. Moreover, tasquinimod significantly reduced IL-10 expression, which is a well-known anti-inflammatory cytokine that induces immunosuppression and is associated with M2 polarization.[26 27] Using flow cytometry on tasquinimod-treated myeloid cells, we observed a decrease in CD206 expression within the macrophage population (CD11b$^+$ F4/80$^+$), again confirming a shift in their polarization state (figure 3D).

Since tasquinimod reduced IL-10 expression, a cytokine reported to dictate the immunosuppressive function of MDSC, we further evaluated the impact of recombinant IL-10 on tasquinimod-mediated T cell proliferation in vitro. We found that the addition of IL-10 significantly hampered the T cell proliferating capacity, particularly at the 1/1 MDSC-T cell ratio (online supplemental figure S8A).

To evaluate whether the immunomodulating effect of tasquinimod could be mediated by HDAC4 targeting, we repeated the same T cell proliferation assay with/without HDAC inhibitor panobinostat. Although panobinostat was able to increase T cell proliferation in the presence of MDSC; we could clearly observe a more pronounced T cell proliferative effect in coculture assays with tasquinimod (online supplemental figure S8B). These data suggest that both HDAC4 and S100A9 targeting in myeloid cells could be responsible for the increased T cell proliferation in vitro.

Altogether, these data demonstrate a clear effect of tasquinimod on the myeloid cell phenotype and function, resulting in a reduced immunosuppressive capacity and increased T cell activating potential.

Short-term tasquinimod treatment of 5TMM mice modulates the myeloid cell phenotype and increases T cell activation

To evaluate whether the observed in vitro effects on myeloid cells could also be found in vivo, 5TGM1 MM mice were treated for a 10-day period with 30 mg/kg tasquinimod (figure 4A). Mice were treated at an early stage after MM cell inoculation (at day 1), as we know the myeloid cell population is already skewed toward an immunosuppressive phenotype the first week after MM injection.[23] Various myeloid cell subtypes were investigated by flow cytometry including monocytic myeloid

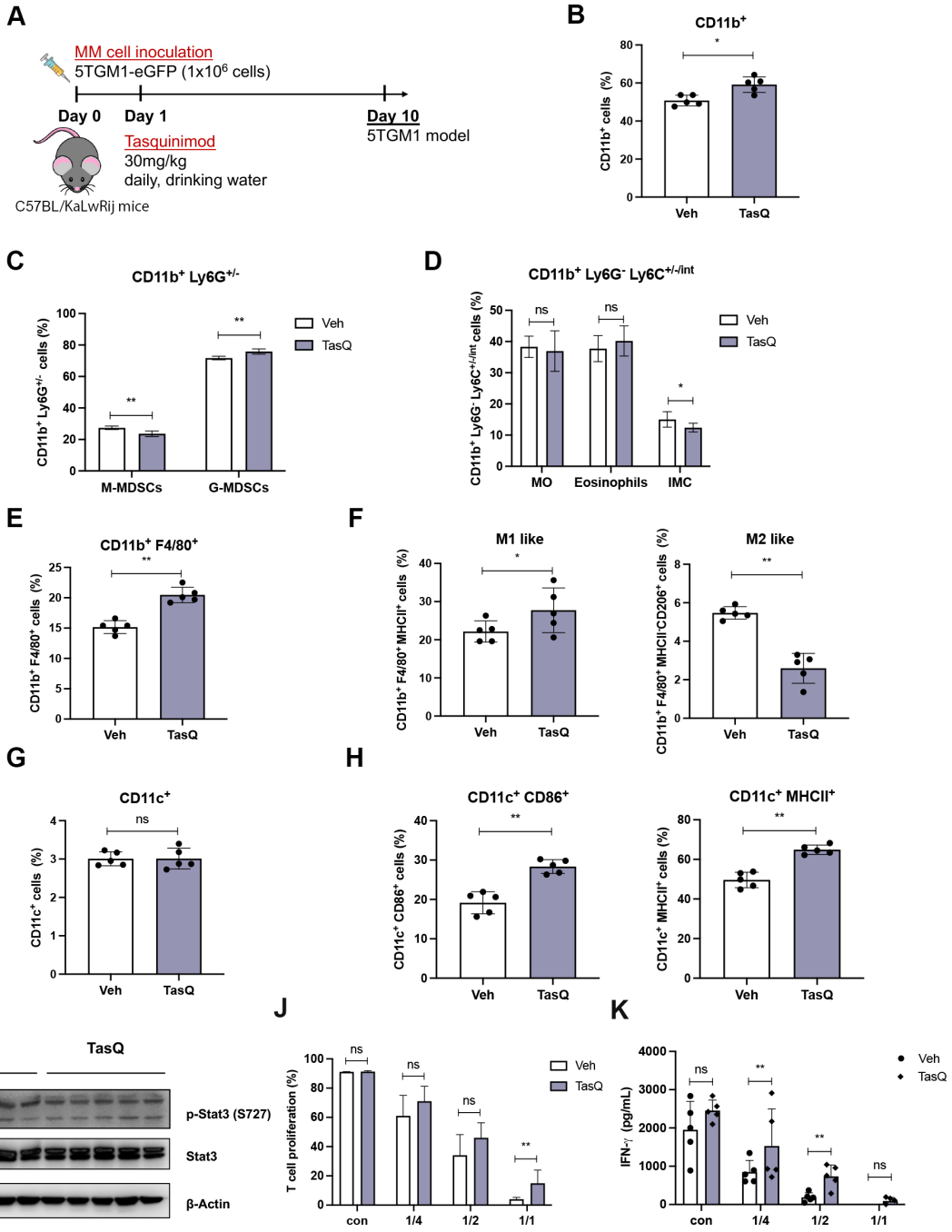

Figure 4 Short-term tasquinimod treatment of 5TMM mice modulates the myeloid cell phenotype and increases T cell activation. (A) 6-week-old C57BL/KaLwRij mice were inoculated with 1.0×10^6 5TGM1-eGFP cells on day 0 and treatment with tasquinimod (TasQ, 30 mg/kg in daily drinking water) started on day 1 (n=5/group). At day 10, all mice were sacrificed to investigate immune cell populations using flow cytometry. (B) The effect of tasquinimod on the percentage of $CD11b^+$ cells in tasquinimod-treated mice compared with vehicle mice. (C) The percentage of monocytic MDSCs (M-MDSCs) ($CD11b^+$, $Ly6G^-$) and granulocytic MDSCs (G-MDSCs) ($CD11b^+$, $Ly6G^+$) in tasquinimod-treated mice compared with vehicle mice. (D) In the $CD11b^+Ly6G^{low}$ population three MDSC subtypes were distinguished based on Ly6C ($Ly6C^{hi}$ inflammatory monocytes (MO), $Ly6C^{intermediate}$ eosinophils, and $Ly6C^{low}$ immature myeloid cells (IMC)). (E) The percentage $F4/80^+$ cells within the $CD11b^+$ cell population in vehicle and tasquinimod-treated mice. (F) Frequency of $CD11b^+$ $F4/80^+$ $MHCII^+$ cells (M1 like) and $CD11b^+$ $F4/80^+$ $MHCII^-$ $CD206^+$ cells (M2 like) in the 5TGM1 model±tasquinimod treatment for 10 days. (G) Percentage of total $CD11c^+$ cells. (H) Percentage of $CD86^+$ $MHCII^+$ $CD11c^+$ cells in 5TGM1 model±tasquinimod treatment for 10 days. (I) $CD11b^+$ cells were sorted from the BM of 5TGM1 mice treated with tasquinimod or vehicle, followed by western blot for p-Stat3. (J) T cells were stimulated with CD3/CD28 in the presence of $CD11b^+$ cells from mice treated with tasquinimod or vehicle (at indicated ratios) and proliferation was measured by CFSE incorporation using flow cytometry. (K) IFN-γ ELISA of supernatant of naïve spleen cells cocultured with BM $CD11b^+$ cells of mice treated with tasquinimod or vehicle (n=5/group). *p<0.05, **p<0.01, Mann-Whitey U test, Error bars indicate SD. BM, bone marrow; CFSE, carboxyfluorescein succinimidyl ester; MACS, magnetic-activated cell sorting; MDSCs, myeloid-derived suppressor cells.

cells (CD11b$^+$, Ly6G$^-$, Ly6C$^{high, intermediate, low}$), granulocytic myeloid cells (CD11b$^+$, Ly6G$^+$), macrophages (CD11b$^+$, F4/80$^+$, CD206/MHCII) and DCs (CD11c$^+$, CD86/MHCII$^+$) (online supplemental figure S9).[28] Short-term tasquinimod therapy did not result in an altered homing of the MM cells to the bone marrow (online supplemental figure S10), however, we could clearly observe a significant increase in the total percentage of CD11b$^+$ cells (figure 4B). While the monocytic and immature myeloid cell population (CD11b$^+$, Ly6G$^-$, Ly6C^{low}) slightly decreased (figure 4C,D), we observed an increase in the macrophage population (CD11b$^+$, F4/80$^+$), which displayed a more M1-like proinflammatory phenotype (MHCII$^+$) and a reduced expression of M2 marker CD206 (figure 4E,F). As STAT3 signaling in myeloid cells is linked to their immunosuppressive capacity, we analyzed this specific signaling pathway on bone marrow derived MACS-sorted CD11b$^+$ cells. CD11b$^+$ cells of tasquinimod-treated mice demonstrated reduced p-STAT33 expression compared with control CD11b$^+$ cells (figure 4I). Moreover, tasquinimod significantly increased the DC maturation marker MHC class II and costimulatory molecule CD86, suggesting a more mature phenotype of DCs (figure 4G,H).

To investigate whether in vivo tasquinimod therapy could inhibit the immunosuppressive capacity of myeloid cells, CD11b$^+$ cells were isolated from vehicle and tasquinimod-treated MM-bearing mice followed by a T cell proliferation assay. T cells cocultured in vitro with MDSCs of tasquinimod-treated mice showed an increase in T cell proliferation that was accompanied by an increased IFN-γ secretion compared with T cells cocultured in vitro with MDSCs of vehicle-treated mice (figure 4J,K).

Tasquinimod decreases tumor burden and significantly prolongs median survival of 5TMM mice

To address the impact of tasquinimod on tumor load and survival in vivo, we used the 5TGM1 and 5T33 immunocompetent murine models, characterized by a moderate (±35 days) and rapid (±21 days) tumor growth in the bone marrow respectively. Daily treatment with tasquinimod (30 mg/kg) resulted in a significant reduction in tumor load in both 5TGM1 (reduced GFP$^+$ tumor cells) and 5T33MM mice (reduction in % bone marrow plasmacytosis) (figure 5A,B). In addition, we observed a decrease in the serum M-protein levels of tasquinimod-treated mice compared with vehicle mice in the 5TGM1 model (figure 5C). As c-MYC downregulation was previously associated with the direct anti-MM effects of tasquinimod in vitro, we investigated c-MYC expression in purified MM cells from vehicle and tasquinimod-treated 5TGM1 and 5T33 myeloma mice (>90% purity of MM cells). Interestingly, our data confirmed a tasquinimod-mediated downregulation of c-MYC expression in the tumor cells of both models, potentially linked to HDAC4 targeting (figure 5D). In addition, we detected a significant increase in IFN-γ levels in tasquinimod-treated 5T33MM mice, indicative for increased T cell activation (figure 5E).

In a last step, we also investigated the impact of tasquinimod therapy on the survival of MM-bearing mice. 5TGM1-eGFP mice were treated as described above and animals were sacrificed when they showed humane endpoint signals (eg, significant weight loss, hindlimb paralysis). The median survival of animals receiving tasquinimod therapy significantly increased compared with the control group (36 days for tasquinimod vs 31 days for vehicle group, p<0.001), again illustrating its therapeutic potential in MM (figure 5F).

Tasquinimod therapy resulted in increased trabecular bone volume in vivo

As S100A8/S100A9 expression has been linked to increased bone resorptive activity of mature osteoclasts, but reduced monocyte-to-osteoclast differentiation[29]; we assessed the impact of tasquinimod therapy on osteolytic lesions. Comparable to the human situation, 5TGM1 MM mice develop lytic bone lesions which can be visualized radiographically using micro-CT (figure 6A). Tasquinimod-treated mice demonstrated an increased bone volume fraction (BV/TV) (figure 6B), trabecular number (Tb.N.) (figure 6C), surface density (BS/TV) (figure 6D) and trabecular thickness (Tb.Th.) (figure 6E), while no effect could be observed on the cortical bone volume (C.BV.) (figure 6F).

These data provide evidence for the use of S100A9 inhibitor tasquinimod in the treatment of MM-induced bone disease, particularly mediated by effects on the trabecular bone mass.

DISCUSSION

We demonstrate here the dual therapeutic effects of the small molecule inhibitor tasquinimod in MM, by remodeling the immunosuppressive microenvironment and by directly targeting MM cell proliferation. We found that tasquinimod reduced the proliferation and colony growth of MM cells, in an S100A9-independent manner, which was associated with a downregulation of pSTAT3 and c-MYC. Additionally, we observed a shift in the immune cell phenotypes, including an increase in M1-like proinflammatory macrophages (MHCII$^+$) and mature DCs, along with increased T cell activation; illustrating its immune activating capacity. Moreover, using immunocompetent mouse models, we demonstrated the therapeutic potential of tasquinimod in MM, illustrated by a reduction in tumor load, increased bone volume and prolonged survival of MM-bearing mice.

Our findings provide new insights on how tasquinimod modulates the bone marrow niche and directly affects tumor progression in MM. Prior research in solid tumors already demonstrated an impact of tasquinimod on immune activation through modulation of the tumor microenvironment. In both a melanoma and prostate cancer model, they found that tasquinimod reduced the

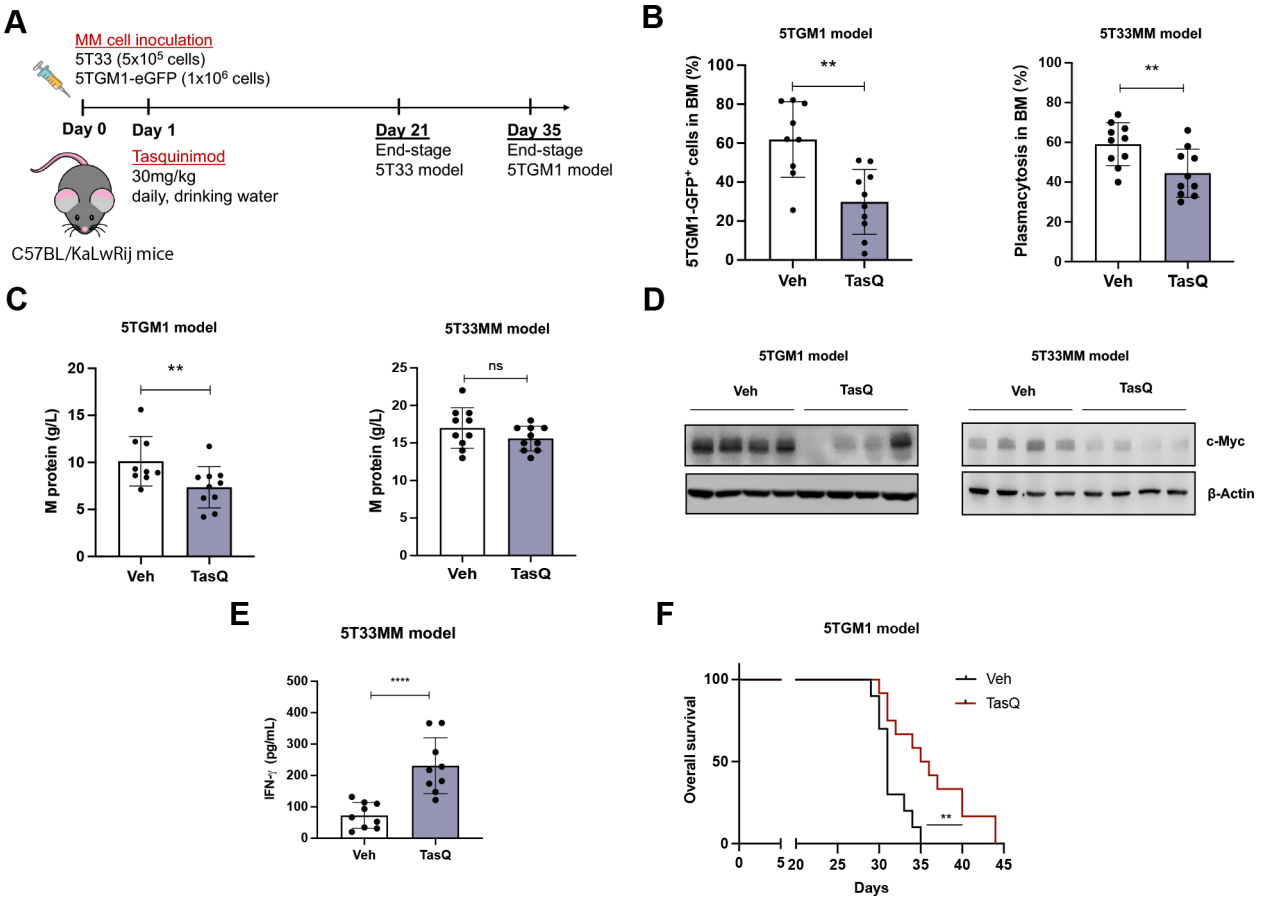

Figure 5 Tasquinimod decreases tumor burden and significantly prolongs median survival of 5TMM mice. (A) 6-week-old C57BL/KaLwRij mice were inoculated with 1.0×10^6 5TGM1-eGFP cells on day 0 for the 5TGM1 model (n=10/group). Six-week-old C57BL/KaLwRij mice were inoculated with 1.0×10^6 5T33vv cells on day 0 for the 5T33MM model (n=10/group). Treatment with tasquinimod (30 mg/kg in daily drinking water) started on day 1. At day 35 (5TGM1 model) or 21 (5T33MM model) all mice were sacrificed. (B) In the 5TGM1 model, teGFP expression was analyzed using flow cytometry to determine the number of tumor cells in the bone marrow. For the 5T33MM model, tumor load was assessed using May-Grunwald Giemsa-stained cytosmears of mononuclear bone marrow cells and the percentage plasma cells was calculated. (C) The M protein was analyzed by serum electrophoresis. (D) MM cells were MACS sorted from the bone marrow of vehicle and tasquinimod-treated mice and c-MYC levels were detected via western blot. (E) Serum IFN-γ concentration in the 5T33MM model was detected using ELISA. (F) Kaplan-Meier survival curves for the 5TGM1 mice treated with/without tasquinimod (n=10/group). **p<0.01, ****p<0.0001, Mann-Whitney U test. Error bars indicate SD. MM, multiple myeloma.

number of tumor-infiltrating MDSCs and M2 polarized macrophages, and was able to impair their suppressive capacity.[30 31] The switch in macrophage polarization was also observed in the 4T1 breast cancer model, where tasquinimod significantly reduced the development of lung metastasis.[32] In contrast to solid tumors, we observed a clear increase in the total number of $CD11b^+$ cells after short-term and long-term treatment with tasquinimod in MM-bearing mice. Notably, this increase was associated with a higher number of M1-like macrophages and more mature DCs, both important players to activate an immune response. While tasquinimod had no direct effect on the T cell number and functionality, it affected the immunosuppressive myeloid cell population which resulted in increased T cell proliferation and IFN-γ secretion. Previous work by our group already showed a high expression of S100A9 and its receptors TLR4 (and RAGE) on myeloid cells, while the expression was low or even absent on T cells and MM cells; suggesting that the effect of tasquinimod is particularly attributed to targeting of the myeloid cell population.[15] All these data illustrate the immune activating capacity of tasquinimod in MM models, not by depleting the immunosuppressive myeloid cells but by switching their phenotype into a less suppressive and more proinflammatory state.

Although the immunoactivating properties of tasquinimod are linked with S100A9-targeting, it has been shown that tasquinimod suppresses tumor angiogenesis and tumor growth by allosteric binding to the regulatory Zn^{2+} binding domain of HDAC4.[10 33] In MM, HDAC4 was previously described as a regulator of tumor cell growth and survival; while HDAC5, 7 and 9 had no effect on MM cell proliferation.[34] Tasquinimod had no effect on MM cell apoptosis, however, we could clearly observe a reduction in MM cell proliferation; while HS-5 stromal cells remained unaffected.[35] As MM cells are S100A9

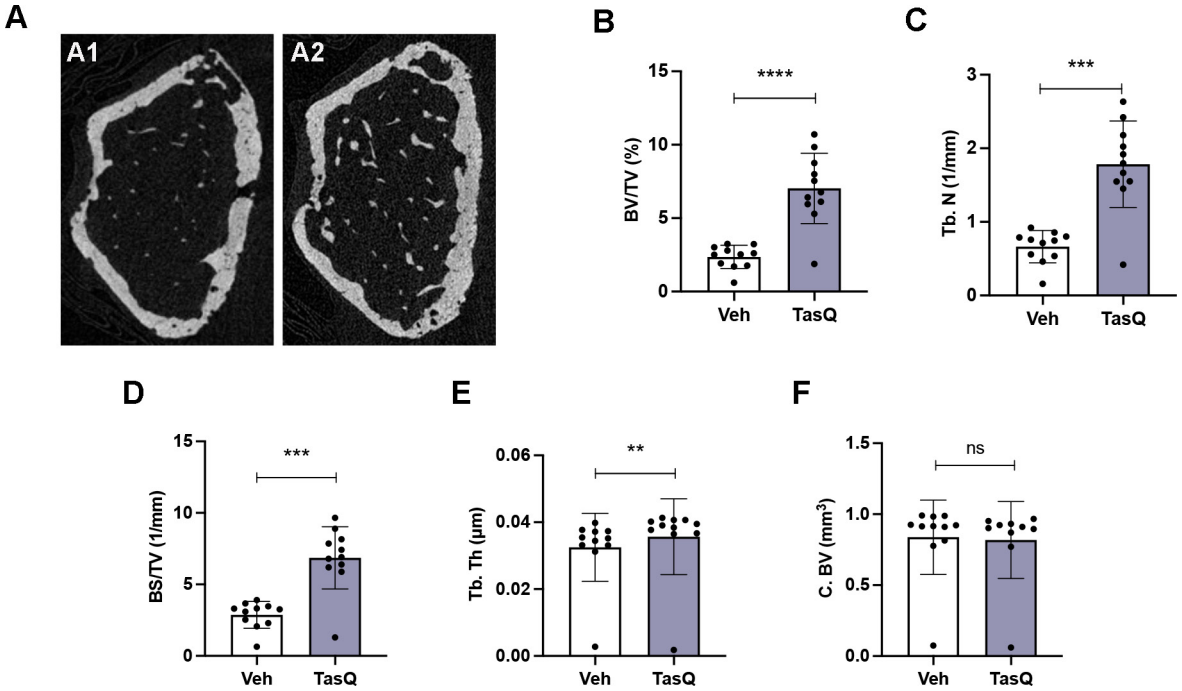

Figure 6 Tasquinimod therapy resulted in increased trabecular bone volume in vivo. (A) Three-dimensional reconstructions of micro-CT scans of the representative femur from vehicle (A1) and tasquinimod-treated 5TGM1 mice (A2). (B) Percentage of bone volume over total volume or bone volume fraction (BV/TV). (C) Trabecular number (Tb.N). (D) Surface density (BS/TV). (E) Trabecular thickness (Tb. Th). (F) Cortical bone volume (C. BV). **p<0.01, ***p<0.001, ****p<0.0001, Mann-Whitney U test. Error bars indicate SD, n=10 per group.

negative and HDAC4 positive, the effect of tasquinimod is potentially attributed to HDAC4-mediated targeting of the tumor cells.[12] HDAC4 is a potent transcriptional repressor and regulates the expression of numerous genes (eg, ATF4, NF-kB) which are potentially involved in the anti-MM effect. Previous studies already demonstrated a close interplay between HDAC and c-MYC/p27 expression in cancer.[24 36] Accordingly, our data supported this notion as tasquinimod-mediated targeting of MM cells resulted in reduced c-MYC and increased p27 expression in vitro.

Tasquinimod-mediated antitumor effects were further evaluated in vivo and demonstrated a significant impact on tumor load, osteolytic lesions and a prolonged survival of MM-bearing mice. Whether the antitumor effect was attributed to the immune-activating potential of tasquinimod or to the direct targeting of MM cells (or a combination of both) remains to be elucidated, however, the increase in serum IFN-γ levels (at end-stage) together with the shift of myeloid cell populations (after short-term treatment) points toward the immunostimulating properties of tasquinimod in this cancer model.

Depending on the time of exposure, S100A8/S100A9 proteins were previously reported to stimulate or reduce bone resorption. Exposure of osteoclast precursors to S100A9 strongly inhibited their osteoclastogenic potential, while the addition of S100A8/S100A9 to mature osteoclasts stimulated their bone-resorbing activity.[29 37] Our study clearly demonstrated an increase in the trabecular bone volume after tasquinimod treatment in MM-bearing mice, hence suggesting a therapeutic potential of tasquinimod for treating MM bone disease.

Altogether, this study gives insights in potential further combination trials in MM patients. The compound is currently evaluated in a non-randomized phase Ib/IIa for relapsed/refractory MM patients, in combination with a standard MM regimen including ixazomib, lenalidomide, and dexamethasone (IRd) (NCT04405167).[38] In castrate-resistant prostate cancer trials (NCT01732549, NCT01234311), the compound demonstrated efficacy and a favorable safety profile.[39] As tasquinimod suppresses the immunosuppressive microenvironment, a combination therapy of this small molecule inhibitor with other immunotherapeutic approaches could provide a promising therapeutic option for MM patients and should be further researched preclinically.

Author affiliations
[1]Laboratory for Hematology and Immunology, Department of Biomedical Sciences, Vrije Universiteit Brussel, Brussels, Belgium
[2]Lab of Cellular and Molecular Immunology, Vrije Universiteit Brussel, Brussels, Belgium
[3]Lab of Dendritic Cell Biology and Cancer Immunotherapy, VIB Center for Inflammation Research, Brussels, Belgium
[4]Department of Clinical Hematology, Universitair Ziekenhuis Gent, Ghent, Belgium
[5]Department of Oncology and Metabolism, Sheffield Myeloma Research Team, University of Sheffield, Sheffield, UK
[6]Department of Clinical Hematology, Universitair Ziekenhuis Brussel, Brussels, Belgium
[7]Active Biotech AB, Lund, Sweden
[8]Center for Medical Genetics, Vrije Universiteit Brussel (VUB), Universitair Ziekenhuis Brussel (UZ Brussel), Brussels, Belgium

[9]Laboratory for Molecular and Cellular Therapy, Department of Biomedical Sciences, Vrije Universiteit Brussel, Brussels, Belgium

Acknowledgements The authors thank Carine Seynaeve and Charlotte Van De Walle for excellent laboratory assistance in microscopy, isolation and staining.

Contributors Study design: KDV and RF; methodology and investigation: RF, HS, CM, EV, NV and HE; resources: KDV, MT and HE; bioinformatic analysis: KM, PV and RF; formal analysis: RF and KDV; writing-original draft preparation: RF and KDV; manuscript editing: HS, NV, EV, AM, EDB, EM, HE, AC, NDB, PV, DH, MT, HE, KV, KM and KB; Supervision: KDV, KM and KB; Guarantor: KDV. The author(s) read and approved the final manuscript.

Funding This study was supported by the VUB spearhead research programs and the Wetenschappelijk Fonds Willy Gepts of Universitair Ziekenhuis Brussel. KDV is postdoctoral fellow of FWO Vlaanderen (12I0921N). NV and CM are predoctoral fellows of FWO Vlaanderen (1159622N, 1103223N). RF was supported by a China Scholarship Council (CSC)-VUB scholarship.

Competing interests This study was in part funded by Active Biotech.

Patient consent for publication Not applicable.

Ethics approval All experiments were reviewed and approved by the Ethical Committee for Animal Experiments of the Vrije Universiteit Brussel (license no. LA1230281, ethical number 21-281-1).

Provenance and peer review Not commissioned; externally peer reviewed.

Data availability statement All data relevant to the study are included in the article or uploaded as online supplemental information.

ORCID iDs
Rong Fan http://orcid.org/0000-0003-1032-4546
Nathan De Beule http://orcid.org/0000-0002-8786-9168
Ken Maes http://orcid.org/0000-0001-8906-2790
Kim De Veirman http://orcid.org/0000-0002-1313-6121

REFERENCES

1 NWCJ vandeD, Pawlyn C, Yong KL. Multiple myeloma. *Lancet* 2021;397:410–27.
2 Kawano Y, Moschetta M, Manier S, *et al*. Targeting the bone marrow microenvironment in multiple myeloma. *Immunol Rev* 2015;263:160–72.
3 Gooding S, Edwards CM. New approaches to targeting the bone marrow microenvironment in multiple myeloma. *Curr Opin Pharmacol* 2016;28:43–9.
4 Labani-Motlagh A, Ashja-Mahdavi M, Loskog A. The tumor microenvironment: a milieu hindering and obstructing antitumor immune responses. *Front Immunol* 2020;11:940–40.
5 Minnie SA, Hill GR. Immunotherapy of multiple myeloma. *J Clin Invest* 2020;130:1565–75.
6 Lakshman A, Kumar SK. Chimeric antigen receptor T-cells, bispecific antibodies, and antibody-drug conjugates for multiple myeloma: an update. *Am J Hematol* 2022;97:99–118.
7 Ahn S, Leblay N, Neri P. Understanding the mechanisms of resistance to T cell-based immunotherapies to develop more favorable strategies in multiple myeloma. *Hemasphere* 2021;5:e575.
8 Lindo L, Wilkinson LH, Hay KA. Befriending the Hostile tumor microenvironment in car T-cell therapy. *Front Immunol* 2020;11:618387.
9 Osanto S, van Poppel H, Burggraaf J. Tasquinimod: a novel drug in advanced prostate cancer. *Future Oncol* 2013;9:1271–81.
10 Pelletier M, Simard J-C, Girard D, *et al*. Quinoline-3-carboxamides such as tasquinimod are not specific inhibitors of S100A9. *Blood Adv* 2018;2:1170–1.
11 Källberg E, Vogl T, Liberg D, *et al*. S100A9 interaction with TLR4 promotes tumor growth. *PLoS One* 2012;7:e34207–e07.
12 Isaacs JT, Antony L, Dalrymple SL, *et al*. Tasquinimod is an allosteric modulator of HDAC4 survival signaling within the compromised cancer microenvironment. *Cancer Res* 2013;73:1386–99.
13 Olsson A, Björk A, Vallon-Christersson J, *et al*. Tasquinimod (ABR-215050), a quinoline-3-carboxamide anti-angiogenic agent, modulates the expression of thrombospondin-1 in human prostate tumors. *Mol Cancer* 2010;9:107.
14 Gupta N, Al Ustwani O, Shen L, *et al*. Mechanism of action and clinical activity of tasquinimod in castrate-resistant prostate cancer. *Onco Targets Ther* 2014;7:223–34.
15 De Veirman K, De Beule N, Maes K, *et al*. Extracellular S100A9 protein in bone marrow supports multiple myeloma survival by stimulating angiogenesis and cytokine secretion. *Cancer Immunol Res* 2017;5:839–46.
16 Dobin A, Davis CA, Schlesinger F, *et al*. STAR: ultrafast universal RNA-seq aligner. *Bioinformatics* 2013;29:15–21.
17 Gentleman RC, Carey VJ, Bates DM, *et al*. Bioconductor: open software development for computational biology and bioinformatics. *Genome Biol* 2004;5:R80.
18 Love MI, Huber W, Anders S. Moderated estimation of fold change and dispersion for RNA-seq data with DESeq2. *Genome Biol* 2014;15:550.
19 De Bruyne E, Bos TJ, Schuit F, *et al*. IGF-1 suppresses Bim expression in multiple myeloma via epigenetic and posttranslational mechanisms. *Blood* 2010;115:2430–40.
20 De Veirman K, Puttemans J, Krasniqi A, *et al*. CS1-specific single-domain antibodies labeled with actinium-225 prolong survival and increase CD8+ T cells and PD-L1 expression in multiple myeloma. *Oncoimmunology* 2021;10:2000699.
21 Oyajobi BO, Muñoz S, Kakonen R, *et al*. Detection of myeloma in skeleton of mice by whole-body optical fluorescence imaging. *Mol Cancer Ther* 2007;6:1701–8.
22 Faict S, Muller J, De Veirman K, *et al*. Exosomes play a role in multiple myeloma bone disease and tumor development by targeting osteoclasts and osteoblasts. *Blood Cancer J* 2018;8:105.
23 De Veirman K, Van Ginderachter JA, Lub S, *et al*. Multiple myeloma induces Mcl-1 expression and survival of myeloid-derived suppressor cells. *Oncotarget* 2015;6:10532–47.
24 Hirano M, Imai Y, Kaito Y, *et al*. Small-molecule HDAC and Akt inhibitors suppress tumor growth and enhance immunotherapy in multiple myeloma. *J Exp Clin Cancer Res* 2021;40:110.
25 Veglia F, Sanseviero E, Gabrilovich DI. Myeloid-derived suppressor cells in the era of increasing myeloid cell diversity. *Nat Rev Immunol* 2021;21:485–98.
26 Berardi S, Ria R, Reale A, *et al*. Multiple myeloma macrophages: pivotal players in the tumor microenvironment. *J Oncol* 2013;2013:1–6.
27 Shapouri-Moghaddam A, Mohammadian S, Vazini H, *et al*. Macrophage plasticity, polarization, and function in health and disease. *J Cell Physiol* 2018;233:6425–40.
28 Bassler K, Schulte-Schrepping J, Warnat-Herresthal S, *et al*. The myeloid cell Compartment-Cell by cell. *Annu Rev Immunol* 2019;37:269–93.
29 Di Ceglie I, Blom AB, Davar R, *et al*. The alarmin S100A9 hampers osteoclast differentiation from human circulating precursors by reducing the expression of RANK. *Faseb J* 2019;33:10104–15.
30 Shen L, Sundstedt A, Ciesielski M, *et al*. Tasquinimod modulates suppressive myeloid cells and enhances cancer immunotherapies in murine models. *Cancer Immunol Res* 2015;3:136–48.
31 Olsson A, Nakhlé J, Sundstedt A, *et al*. Tasquinimod triggers an early change in the polarization of tumor associated macrophages in the tumor microenvironment. *J Immunother Cancer* 2015;3:53.
32 Brower V. Tasquinimod treatment for prostate cancer. *Lancet Oncol* 2016;17:e322.
33 Cheng C, Yang J, Li S-W, *et al*. HDAC4 promotes nasopharyngeal carcinoma progression and serves as a therapeutic target. *Cell Death Dis* 2021;12:137.
34 Kikuchi S, Suzuki R, Ohguchi H, *et al*. Class IIa HDAC inhibition enhances ER stress-mediated cell death in multiple myeloma. *Leukemia* 2015;29:1918–27.
35 Ramachandran IR, Lin C, Chase T, *et al*. A novel agent tasquinimod demonstrates a potent anti-tumor activity in pre-clinical models of multiple myeloma. *Blood* 2014;124:5729–29.

36 Nebbioso A, Carafa V, Conte M, *et al*. C-Myc modulation and acetylation is a key HDAC inhibitor target in cancer. *Clin Cancer Res* 2017;23:2542–55.
37 van den Bosch MH, Blom AB, Schelbergen RF, *et al*. Alarmin S100A9 induces proinflammatory and catabolic effects predominantly in the M1 macrophages of human osteoarthritic synovium. *J Rheumatol* 2016;43:1874–84.
38 Vogl DT, Nefedova Y, Wileyto EP, *et al*. A phase 1 study of tasquinimod in patients with relapsed or refractory multiple myeloma. *Blood* 2020;136:17–18.
39 Mehta AR, Armstrong AJ. Tasquinimod in the treatment of castrate-resistant prostate cancer - current status and future prospects. *Ther Adv Urol* 2016;8:9–18.

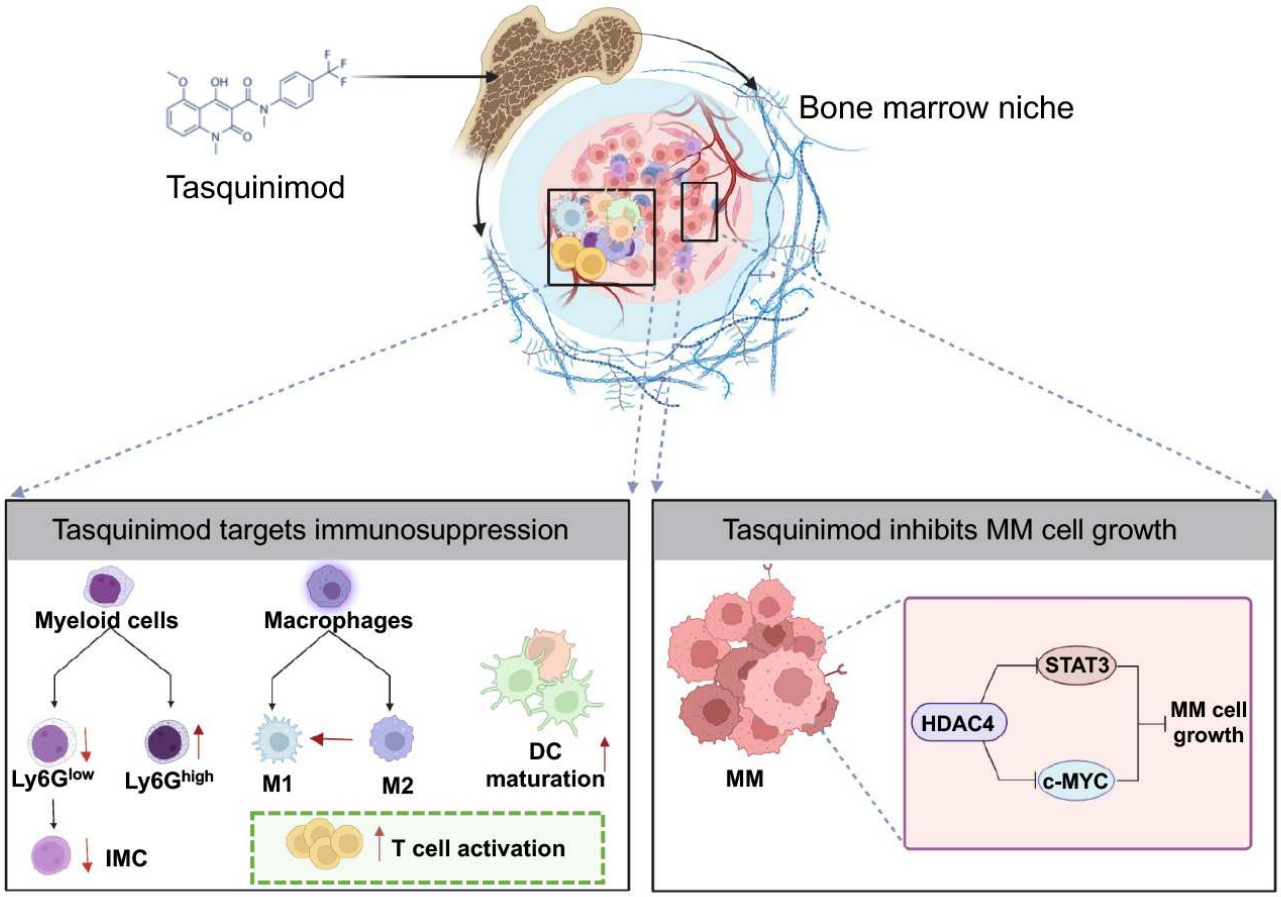

Tasquinimod Suppresses Tumor Cell Growth and Bone Resorption by Targeting Immunosuppressive Myeloid Cells and Inhibiting c-MYC Expression in Multiple Myeloma

Rong Fan[1], Hatice Satilmis[1], Niels Vandewalle[1], Emma Verheye[1,2], Philip Vlummens [1,3], Anke Maes[1], Catharina Muylaert[1], Elke De Bruyne[1], Eline Menu[1], Holly Evans[4], Andrew Chantry[4], Nathan De Beule[5], Dirk Hose[1], Marie Törngren[6], Helena Eriksson[6], Karin Vanderkerken[1], Ken Maes[7], Karine Breckpot[8], Kim De Veirman[1]

Supplementary Material and Methods

Reagents

Recombinant mouse IL-10 (#575804, biolegend) was used at a concentration of 100 ng/mL for the T cell suppression assay. The HDAC inhibitor panobinostat (LBH589, Novartis Pharmaceuticals) was purchased from Selleckchem (East Hanover, NJ) and prepared as a 10 mM stock solution in dimethylsulfoxide and stored at −80°C.

Gene expression data

The online webtool GenomicScape (http://genomicscape.com/microarray/survival.php) was consulted for the microarray data of the TT2 cohort (accession number: GSE204225, http://www.ncbi.nlm.nih.gov/geo/). Gene expression of HDAC4 was analyzed in bone marrow plasma cells (BMPCs) of healthy individuals (n = 22) and in patient samples at different MM substages including monoclonal gammopathy of undetermined clinical significance (MGUS) (n = 44), smoldering multiple myeloma (SMM) (n = 12) and $CD138^+$ cells of newly diagnosed MM patients (n = 345) and primary MM cell lines (n = 23). Gene expression data were normalized with the MAS5 algorithm.

Cell culture

MM cell lines were seeded at a concentration of 2.5×10^5 cells/mL with different concentrations of tasquinimod (10, 25 µM) for 3 days and 5 days in 1% FCS RPMI medium. Apoptosis was measured by flow cytometry using the Annexin-V/7-AAD staining. MM cell lines were seeded at a concentration of 5.0×10^5 cells/mL with different concentrations of panobinostat (0.5, 1 µM) for 6 h and 24 h.

Cell viability

$CD11b^+$ cells were sorted from 5TGM1 model and 5T33MM model by CD11b microbeads and seeded in a white, opaque 96-well plate. The following day, cells were treated with tasquinimod and cell viability was measured at 24 h post-treatment using the CellTiter-Glo® Luminescent Cell Viability Assay (Promega, G7573)

Fan R, *et al. J Immunother Cancer* 2023; 11:e005319. doi: 10.1136/jitc-2022-005319

according to manufacturer's instructions. Microplate luminescence was measured using a CLARIOstar (BMG Labtech) plate reader. All data were normalized to non-treated controls.

Supplementary Table 1. Mouse primer sequences of genes evaluated by real-time quantitative PCR

Gene		**Primer sequence 5'-3'**
Abl	Forward	CCG TGG GTG CCA CTA TAT TT
	Reverse	GGG CAC AGT GGT GAA CTA TT
Arg1	Forward	ACA GCA AAG CAG ACA GAA CTA
	Reverse	GAA AGG AAC TGC TGG GAT ACA
Fizz1	Forward	CCC AGT GAA TAC TGA TGA GAC C
	Reverse	GGA GGG ATA GTT AGC TGG ATT G
Mrc1	Forward	GGA ATC AAG GGC ACA GAG TTA
	Reverse	TTC CAT CTG CTC CAC AAT CC
Nos2	Forward	GGA ATC TTG GAG CGA GTT GT
	Reverse	CCT CTT GTC TTT GAC CCA GTA G
Stab1	Forward	ACG GGA AAC TGC TTG ATG TC
	Reverse	ACT CAG CGT CAT GTT GTC CA
Tnfa	Forward	CTA CCT TGT TGC CTC CTC TTT
	Reverse	GAG CAG AGG TTC AGT GAT GTA G
IL10	Forward	TTG AAT TCC CTG GGT GAG AAG
	Reverse	TCC ACT GCC TTG CTC TTA TTT
c-Myc	Forward	GCT GTT TGA AGG CTG GAT TTC
	Reverse	GAG TCG TAG TCG AGG TCA TAG T

Supplementary Table 2. Differentially expressed genes in LP-1 cells treated with tasquinimod. Using RNA sequencing, we identified a list of upregulated and downregulated genes in LP-1 cells treated with tasquinimod (25 µM) for 6 h and 24 h (padj ≤ 0.05 & ｜log2FoldChange｜ ≥ 1) (n=3).

Up regulated genes in TasQ treated LP-1 (6 h)													
Ensembl ID	Gene symbol	baseMean	log2FoldChange	lfcSE	stat	pvalue	padj	Cnt1	Cnt2	Cnt3	Tas1	Tas2	Tas3
ENSG00000143153	ATP1B1	103.621196	1.018170392	0.19703	5.16752	2.37E-07	4.03E-06	69.38256	72.4779	64.0296	143.197	118.881	153.76
ENSG00000125266	EFNB2	86.3883412	1.035125581	0.21339	4.85077	1.23E-06	1.79E-05	64.20476	55.4909	50.5022	127.611	113.927	106.594
ENSG00000010704	HFE	104.822284	1.08717393	0.21785	4.99036	6.03E-07	9.48E-06	67.31144	57.7558	75.7533	106.18	143.647	178.286
ENSG00000154309	DISP1	64.3172858	1.102929222	0.24203	4.55691	5.19E-06	6.59E-05	41.42243	39.6364	41.4839	91.5681	81.2351	90.5578
ENSG00000050405	LIMA1	86.8832765	1.174777021	0.2192	5.35946	8.35E-08	1.55E-06	43.49355	50.961	64.9314	118.844	131.759	111.311
ENSG00000076641	PAG1	354.290158	1.307707212	0.11141	11.7373	8.20E-32	1.80E-29	187.4365	220.831	203.812	513.366	521.094	479.202
ENSG00000196083	IL1RAP	83.2898715	1.415285922	0.222	6.37525	1.83E-10	5.31E-09	40.38687	44.1662	51.404	116.895	112.937	133.95
ENSG00000164741	DLC1	74.4918423	1.448455883	0.23361	6.20023	5.64E-10	1.50E-08	39.35131	41.9013	38.7785	104.232	100.058	122.63
ENSG00000197019	SERTAD1	59.4743365	1.608127034	0.26411	6.08879	1.14E-09	2.84E-08	25.88902	30.5766	31.5639	95.4646	94.1139	79.2381
Down regulated genes in TasQ treated LP-1 (6 h)													
Ensembl ID	Gene symbol	baseMean	log2FoldChange	lfcSE	stat	pvalue	padj	Cnt1	Cnt2	Cnt3	Tas1	Tas2	Tas3
ENSG00000169245	CXCL10	1555.72273	-1.726671085	0.06807	-25.364	6.22E-142	7.38E-138	2396.287	2307.97	2462.88	782.225	734.088	650.884
ENSG00000168329	CX3CR1	80.4909195	-1.690891097	0.22995	-7.3534	1.93E-13	8.30E-12	125.3028	114.379	128.961	30.198	42.5989	41.5057
ENSG00000168334	XIRP1	465.496837	-1.657655626	0.10225	-16.212	4.14E-59	4.15E-56	716.608	756.488	648.412	225.998	221.911	223.565
ENSG00000183625	CCR3	219.756282	-1.597770032	0.13972	-11.436	2.77E-30	5.39E-28	303.4193	343.138	344.497	110.076	107.983	109.424
ENSG00000076356	PLXNA2	514.954525	-1.388409651	0.09444	-14.701	6.35E-49	4.19E-46	794.275	738.369	703.423	289.316	281.351	282.993
ENSG00000128917	DLL4	245.673963	-1.350305566	0.13494	-10.007	1.43E-23	1.84E-21	385.2286	349.932	323.755	151.964	137.703	125.46
ENSG00000169085	VXN	98.0317411	-1.333117655	0.20855	-6.3922	1.63E-10	4.77E-09	128.4095	157.413	135.274	63.3183	59.4403	44.3356
ENSG00000223863	LINC01805	153.07184	-1.319443666	0.16739	-7.8823	3.21E-15	1.77E-13	225.7522	210.639	219.143	105.206	82.2258	75.4648
ENSG00000232591	LINC02642	56.6622161	-1.20975926	0.26068	-4.6409	3.47E-06	4.56E-05	86.9871	69.0805	81.1642	36.0427	33.6829	33.0159
ENSG00000221869	CEBPD	51.026088	-1.192533363	0.27693	-4.3063	1.66E-05	0.0001819	82.84485	67.948	62.2259	32.1462	32.6922	28.2993
ENSG00000165970	SLC6A5	74.8623777	-1.190963311	0.22891	-5.2027	1.96E-07	3.42E-06	97.3427	107.584	107.317	50.6547	48.5429	37.7324
ENSG00000107984	DKK1	49.7665669	-1.185073346	0.29999	-3.9504	7.80E-05	0.0007194	59.02696	82.6701	65.8332	42.8616	21.7948	26.4127
ENSG00000100368	CSF2RB	130.748422	-1.145159047	0.1747	-6.5549	5.57E-11	1.71E-09	190.5432	171.003	178.561	92.5422	78.2631	73.5782
ENSG00000053918	KCNQ1	54.4190729	-1.119346433	0.26799	-4.1768	2.96E-05	0.0003028	83.88041	70.213	69.4405	33.1204	40.6176	29.2426
ENSG00000178965	ERICH3	214.922947	-1.117761094	0.13701	-8.1583	3.40E-16	2.05E-14	280.6369	294.441	307.522	148.067	126.806	132.063
ENSG00000184828	ZBTB7C	67.6005665	-1.112931413	0.24167	-4.6052	4.12E-06	5.36E-05	88.02266	101.922	87.477	37.991	51.515	38.6757
ENSG00000181291	TMEM132E	277.330627	-1.11026495	0.12427	-8.9342	4.10E-19	3.40E-17	382.1219	412.218	343.595	181.188	169.405	175.456
ENSG00000163823	CCR1	1203.27605	-1.109650045	0.06845	-16.211	4.19E-59	4.15E-56	1699.355	1688.51	1546.63	801.708	742.013	741.442
ENSG00000053108	FSTL4	177.824507	-1.095425979	0.15829	-6.9204	4.50E-12	1.63E-10	201.9343	270.66	254.315	120.792	106.993	112.254
ENSG00000127831	VIL1	222.089259	-1.07598418	0.14052	-7.6574	1.90E-14	8.96E-13	289.957	274.057	339.086	131.507	154.545	143.383
ENSG00000185862	EVI2B	369.016225	-1.030782678	0.10822	-9.5251	1.65E-21	1.79E-19	478.429	483.563	523.96	263.989	237.761	226.395

Up regulated genes in TasQ treated LP-1 (24 h)													
Ensembl ID	Gene symbol	baseMean	log2FoldChange	lfcSE	stat	pvalue	padj	Cnt1	Cnt2	Cnt3	Tas1	Tas2	Tas3
ENSG00000139112	GABARAPL1	38.3711148	1.094614799	0.31661	3.45729	0.0005456	0.0039602	24.33034	24.4594	24.7579	45.0197	58.41	53.2493
ENSG00000084444	FAM234B	38.3419731	1.087872499	0.31504	3.45311	0.0005542	0.0040157	26.54219	25.4001	21.7869	48.3139	54.7594	53.2493
ENSG00000144642	RBMS3	38.3906879	1.200500052	0.32691	3.67228	0.0002404	0.0019633	17.6948	29.1631	22.7772	46.1178	52.9341	61.6571
ENSG00000084764	MAPRE3	35.7753684	1.285215457	0.33334	3.85558	0.0001155	0.0010567	22.11849	24.4594	15.845	51.608	51.1088	49.5125
ENSG00000204397	CARD16	38.9500164	1.047412393	0.32858	3.18768	0.0014342	0.0088204	25.43627	31.9854	18.816	45.0197	64.7986	47.6441
ENSG00000130589	HELZ2	44.7308589	1.02031668	0.30959	3.29574	0.0009816	0.0064715	29.85997	24.4594	34.661	42.8236	71.1872	65.3939
ENSG00000143603	KCNN3	39.9964207	1.667010993	0.35299	4.7225	2.33E-06	3.40E-05	11.05925	28.2224	17.8257	46.1178	63.886	72.8675
ENSG00000122694	GLIPR2	40.7785087	1.212019906	0.34992	3.46372	0.0005328	0.0038849	22.11849	15.0519	36.6416	60.3923	69.3619	41.1047
ENSG00000152778	IFIT5	56.0192944	1.073961253	0.26541	4.0465	5.20E-05	0.0005323	42.02514	37.6298	28.7191	79.059	73.0126	75.6701
ENSG00000185272	RBM11	24.9968283	1.209443943	0.39208	3.0847	0.0020376	0.011871	15.48295	15.9927	13.8644	30.7452	35.5936	38.3021
ENSG00000198133	TMEM229B	22.896663	1.072243037	0.40585	2.64194	0.0082432	0.0370817	14.37702	14.1112	15.845	27.4511	31.0303	34.5653
ENSG00000115596	WNT6	24.9742134	1.024565383	0.3904	2.62439	0.0086804	0.0387148	17.6948	18.8149	12.8741	34.0393	35.5936	30.8286
ENSG00000164440	TXLNB	23.1095368	1.486864327	0.42398	3.50694	0.0004533	0.0033764	12.16517	8.46671	15.845	38.4315	30.1177	33.6311
ENSG00000079931	MOXD1	31.486598	1.027573766	0.35121	2.92581	0.0034357	0.018275	18.80072	22.5779	20.7966	37.3334	51.1088	38.3021
ENSG00000114626	ABTB1	27.6180976	1.009163945	0.38629	2.61246	0.0089892	0.0398996	17.6948	24.4594	12.8741	28.5491	42.8949	39.2363
ENSG00000169851	PCDH7	33.3543784	1.29059107	0.35912	3.59377	0.0003259	0.0025422	18.80072	23.5186	15.845	34.0393	58.41	49.5125
ENSG00000123609	NMI	98.9780823	1.302167082	0.20248	6.43094	1.27E-10	4.68E-09	54.19031	51.741	65.3608	142.745	136.899	142.932
ENSG00000126821	SGPP1	98.7357042	1.030442916	0.21124	4.87814	1.07E-06	1.71E-05	50.87254	83.7264	59.4189	130.667	135.073	132.656
ENSG00000212443	SNORA53	86.940508	1.182301894	0.24177	4.89028	1.01E-06	1.63E-05	40.91921	46.0965	72.293	115.294	101.305	145.735
ENSG00000168234	TTC39C	108.035083	1.397721754	0.19968	6.99969	2.57E-12	1.26E-10	60.82586	55.504	62.3898	135.059	158.802	175.629
ENSG00000137177	KIF13A	65.0820315	2.083882597	0.26447	7.87937	3.29E-15	2.60E-13	24.33034	23.5186	26.7385	98.8238	104.043	113.038
ENSG00000173530	TNFRSF10D	158.126012	1.023609848	0.16072	6.36871	1.91E-10	6.86E-09	103.9569	111.949	97.0508	196.55	229.99	209.26
ENSG00000184500	PROS1	155.449464	1.13167493	0.17774	6.36691	1.93E-10	6.92E-09	79.62658	111.008	101.012	209.726	249.155	182.169
ENSG00000136842	TMOD1	164.547434	1.347966482	0.16243	8.29886	1.05E-16	1.01E-14	94.0036	85.6079	99.0315	238.275	257.369	212.997
ENSG00000105854	PON2	149.826755	1.161267053	0.16487	7.04344	1.88E-12	9.37E-11	96.21545	90.3116	91.109	225.099	192.571	203.655
ENSG00000185112	FAM43A	128.07146	1.082939209	0.18293	5.91984	3.22E-09	8.95E-08	84.05028	82.7856	79.2252	199.844	148.763	173.761
ENSG00000223247	RNU2-64P	123.411963	1.043965427	0.19258	5.42084	5.93E-08	1.27E-06	76.30881	76.2004	89.1283	171.295	134.161	193.379
ENSG00000182568	SATB1	326.140889	1.1039324	0.11648	9.47759	2.60E-21	4.41E-19	211.2316	210.727	200.044	405.178	469.106	460.56
ENSG00000173706	HEG1	315.566323	1.048705617	0.14871	7.05181	1.77E-12	8.92E-11	162.5709	214.49	239.656	342.589	439.901	494.191
ENSG00000129757	CDKN1C	247.077386	1.13441816	0.13693	8.28465	1.18E-16	1.12E-14	171.4183	142.993	150.528	315.138	322.168	380.219
ENSG00000099954	CECR2	232.514568	1.14131831	0.15895	7.18032	6.95E-13	3.71E-11	190.2191	130.764	115.867	288.785	332.207	337.246
ENSG00000076641	PAG1	414.236923	1.053885463	0.10297	10.235	1.38E-24	3.05E-22	266.5279	270.935	270.356	557.805	527.516	592.282
ENSG00000104081	BMF	2184.0285	1.331990767	0.0615	21.6597	4.92E-104	2.28E-100	1143.526	1314.22	1265.62	3000.95	3197.04	3182.81
ENSG00000135925	WNT10A	1146.39434	1.065875055	0.06988	15.2524	1.59E-52	2.75E-49	757.5584	713.085	754.62	1469.18	1615.4	1568.52
ENSG00000159388	BTG2	3761.03942	1.101356129	0.049	22.476	7.13E-112	4.95E-108	2490.542	2294.48	2391.61	5117.97	5219.48	5052.15
Down regulated genes in TasQ treated LP-1 (24 h)													
Ensembl ID	Gene symbol	baseMean	log3FoldChange	lfcSE	stat	pvalue	padj	Cnt1	Cnt2	Cnt3	Tas1	Tas2	Tas3
ENSG00000213262	VDAC2P3	57.7394309	-1.354138043	0.26711	-5.0696	3.99E-07	7.16E-06	88.47398	68.6744	92.0993	30.7452	34.681	31.7627
ENSG00000100368	CSF2RB	57.1941831	-1.508054408	0.26866	-5.6132	1.99E-08	4.75E-07	89.5799	81.8449	82.1961	35.1373	30.1177	24.2892
ENSG00000170442	KRT86	48.7800833	-1.516178725	0.29138	-5.2034	1.96E-07	3.81E-06	71.88511	63.9707	81.2058	23.0589	29.205	23.355
ENSG00000184408	KCND2	46.7007639	-2.228640509	0.33568	-6.6391	3.16E-11	1.27E-09	86.26213	61.1485	83.1864	20.8628	9.12657	19.6182
ENSG00000169085	VXN	63.9637778	-1.712894755	0.26951	-6.3556	2.08E-10	7.39E-09	116.1221	95.9561	82.1961	29.6471	36.5063	23.355
ENSG00000205426	KRT81	55.2654673	-2.318266133	0.29319	-7.907	2.64E-15	2.10E-13	95.10953	91.2523	90.1186	15.3726	18.2531	21.4866
ENSG00000017483	SLC38A5	71.2630185	-1.339466175	0.23771	-5.6348	1.75E-08	4.23E-07	98.4273	95.0153	112.896	42.8236	41.9822	36.4337
ENSG00000165912	PACSIN3	97.1483993	-1.077000373	0.21803	-4.9398	7.82E-07	1.30E-05	129.3932	133.586	132.702	59.2943	82.1391	45.7757
ENSG00000181291	TMEM132E	92.1484108	-1.108695153	0.22173	-5.0003	5.72E-07	9.94E-06	107.2747	123.238	147.557	47.2158	55.6721	71.9333
ENSG00000135333	EPHA7	93.3607836	-1.516470409	0.21986	-6.8974	5.30E-12	2.48E-10	152.6176	115.712	146.567	54.9021	50.1961	40.1705
ENSG00000183625	CCR3	80.0337247	-1.897577666	0.23443	-8.0943	5.76E-16	5.13E-14	139.3465	120.415	118.838	35.1373	33.7683	32.6969
ENSG00000181631	P2RY13	28.4155885	-1.010563421	0.36929	-2.7365	0.0062092	0.0295291	32.07182	47.0373	34.661	19.7648	17.3405	19.6182
ENSG00000153012	LGI2	27.4343776	-1.067358625	0.38008	-2.8082	0.0049812	0.0247027	33.17774	44.2151	33.6707	23.0589	14.6025	15.8814
ENSG00000232480	TGFB2-AS1	24.7186442	-1.682805052	0.42699	-3.9411	8.11E-05	0.0007836	33.17774	47.0373	32.6804	14.2745	14.6025	6.53939
ENSG00000243721	RPL23AP63	28.2751081	-1.101411561	0.38623	-2.8517	0.0043484	0.0221231	32.07182	44.2151	39.6126	12.0785	15.5152	26.1576
ENSG00000128322	IGLL1	26.0535864	-1.023050968	0.38286	-2.6721	0.0075376	0.0344589	33.17774	31.0446	40.6029	16.4706	20.0785	14.9472
ENSG00000232422	KNOP1P4	23.5731254	-1.035439331	0.40485	-2.5576	0.01054	0.0453477	36.49552	29.1631	29.7094	10.9804	17.3405	17.7498
ENSG00000104218	CSPP1	1963.22444	-0.15807164	0.06137	-2.5755	0.0100087	0.0435203	2120.058	2185.35	1906.36	1868.87	1850.87	1847.84
ENSG00000222724	RNU2-63P	23.8606376	-1.522495048	0.41287	-3.6876	0.0002264	0.0018677	40.91921	36.6891	28.7191	10.9804	12.7772	13.0788
ENSG00000212163	SNORD91A	25.6850497	-1.033595069	0.41013	-2.5202	0.0117298	0.0493652	39.81329	36.6891	26.7385	23.0589	9.12657	18.684
ENSG00000264229	RNU4ATAC	32.9343923	-1.039407002	0.34296	-3.0307	0.0024398	0.0137981	50.87254	40.4521	41.5932	23.0589	17.3405	24.2892
ENSG00000164107	HAND2	32.8757747	-1.134042773	0.34761	-3.2624	0.0011047	0.0071171	56.40216	38.5706	40.6029	21.9608	19.1658	20.5524
ENSG00000102924	CBLN1	29.7085901	-1.077588891	0.36622	-2.9425	0.0032561	0.0174747	44.23699	33.8668	42.5835	25.255	16.4278	15.8814
ENSG00000138772	ANXA3	32.5801694	-1.104795578	0.35916	-3.076	0.0020978	0.0121765	48.66069	49.8595	34.661	25.255	13.6899	23.355
ENSG00000103534	TMC5	41.6362064	-1.081108857	0.30544	-3.5395	0.0004009	0.0030442	66.35548	48.9188	54.4673	27.4511	26.467	26.1576
ENSG00000017427	IGF1	3.78E+01	-1.559730689	0.33296	-4.6844	2.808E-06	4.032E-05	67.46141	50.8002708	51.4963691	17.5686749	17.340481	22.4207643
ENSG00000034053	APBA2	36.7593474	-1.16209464	0.33219	-3.4983	0.0004683	0.0034732	58.61401	47.978	45.5545	29.6471	20.0785	18.684
ENSG00000249307	LINC01088	38.386322	-1.125207759	0.3356	-3.3528	0.0008	0.0054284	54.19031	54.5633	49.5157	16.4706	20.0785	35.4995
ENSG00000225536	STIP1P3	33.3462525	-1.053589342	0.36262	-2.9055	0.0036667	0.0192542	49.76661	43.2743	42.5835	10.9804	30.1177	23.355
ENSG00000130775	THEMIS2	254.554687	0.053701128	0.13274	0.40457	0.6857921	0.8343042	207.9138	262.468	278.278	256.942	258.282	263.444
ENSG00000236972	FABP5P1	48.2921759	-1.086400984	0.28721	-3.7826	0.0001552	0.00135	66.35548	69.6152	61.3995	24.1569	38.3316	29.8944
ENSG00000178752	ERFE	43.9908501	-1.002417612	0.29744	-3.3701	0.0007513	0.0051742	59.71993	58.3262	58.4286	21.9608	34.681	30.8286
ENSG00000134461	ANKRD16	152.532906	-1.037190391	0.16686	-6.2158	5.11E-10	1.67E-08	207.9138	210.727	196.082	110.902	82.1391	107.433
ENSG00000027869	SH2D2A	148.127563	-1.174574316	0.17061	-6.8846	5.79E-12	2.67E-10	196.8546	183.445	235.695	90.0395	94.9163	87.8147
ENSG00000168334	XIRP1	156.027216	-1.784304243	0.16754	-10.65	1.74E-26	4.56E-24	258.7864	234.246	232.724	69.1767	72.0999	69.1307
ENSG00000105971	CAV2	193.265902	-1.081689939	0.15739	-6.8728	6.30E-12	2.87E-10	314.0826	245.535	228.763	116.392	127.772	127.051
ENSG00000166428	PLD4	135.077882	-1.214284399	0.17537	-6.9241	4.39E-12	2.06E-10	174.7361	186.268	204.995	86.7453	85.7897	71.9333
ENSG00000081479	LRP2	128.507676	-1.141334282	0.18127	-6.2964	3.05E-10	1.05E-08	174.7361	171.216	185.189	70.2747	95.829	73.8017
ENSG00000026751	SLAMF7	121.344592	-1.815680416	0.18823	-9.6461	5.11E-22	9.45E-20	183.5835	189.09	194.102	56.0002	51.1088	54.1835
ENSG00000155629	PIK3AP1	119.088952	-1.015422554	0.19502	-5.2068	1.92E-07	3.75E-06	186.9013	137.349	154.489	70.2747	72.0999	93.4199
ENSG00000170681	CAVIN4	105.676614	-1.49088379	0.20274	-7.3536	1.93E-13	1.14E-11	165.8887	169.334	132.702	51.608	55.6721	58.8545
ENSG00000161940	BCL6B	266.732862	-1.217678492	0.13736	-8.865	7.65E-19	9.57E-17	431.3106	350.898	336.707	175.687	145.112	160.682
ENSG00000092969	TGFB2	251.169503	-1.203253116	0.12816	-9.389	6.06E-21	9.67E-19	331.7774	365.009	353.542	154.824	153.326	148.538
ENSG00000076356	PLXNA2	322.906739	-1.281544053	0.12014	-10.667	1.46E-26	3.89E-24	406.9803	471.314	494.167	185.569	192.571	186.84
ENSG00000173334	TRIB1	1619.32037	-1.828297046	0.06932	-26.376	2.59E-153	3.60E-149	2528.144	2388.55	2664.94	698.355	669.89	766.043
ENSG00000019991	HGF	1126.40385	-1.373980428	0.07098	-19.358	1.73E-83	4.81E-80	1713.077	1575.75	1587.47	651.139	606.004	624.979
ENSG00000144485	HES6	3520.70392	-1.190273614	0.15181	-7.8404	4.49E-15	3.46E-13	4317.53	4895.64	5473.47	2424.48	2185.81	1827.29

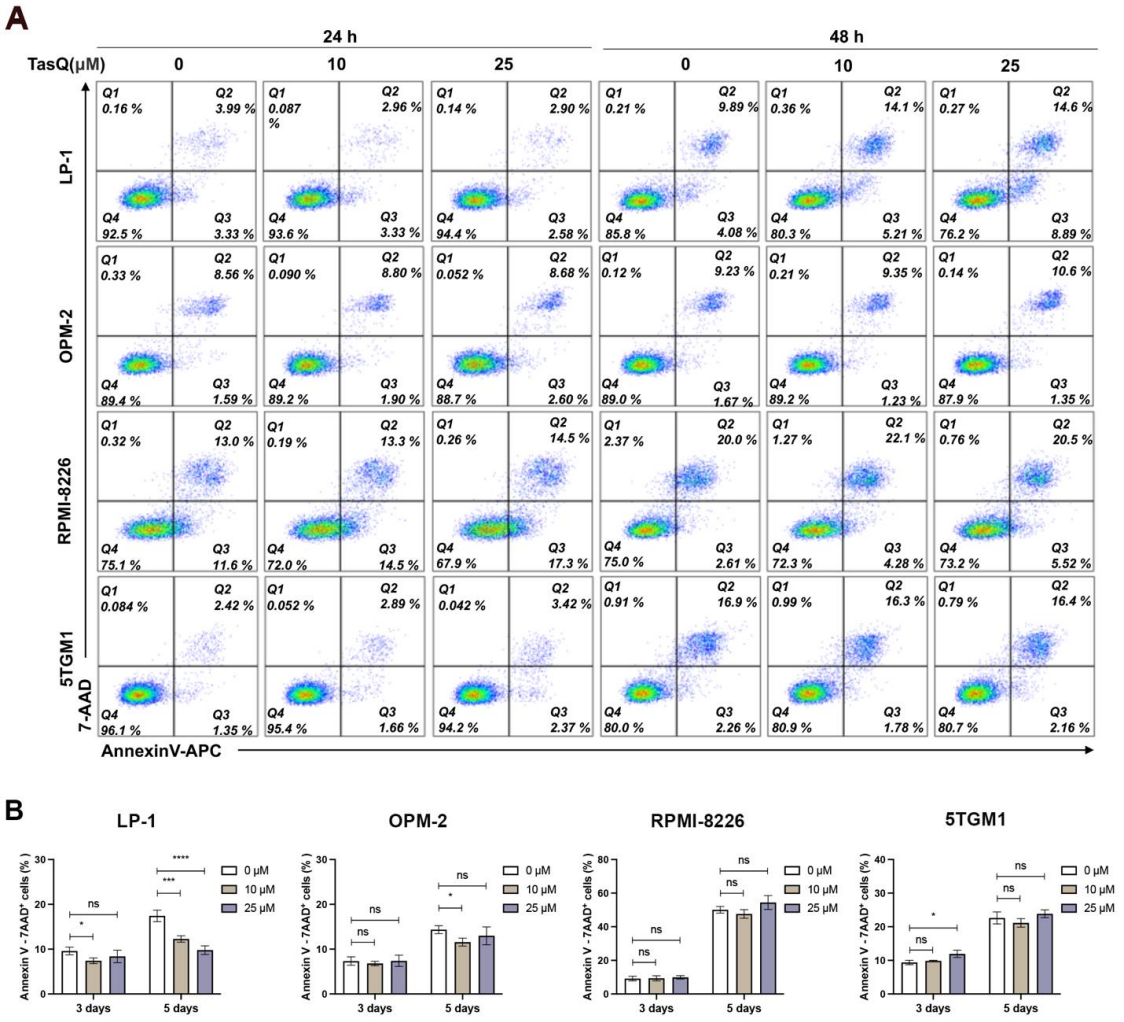

Supplemental Figure 1. Tasquinimod has no effect on MM cell apoptosis. (A) MM cell lines (LP-1, OPM-2, RPMI8226, 5TGM1) were treated with tasquinimod (TasQ) (10, 25 μM) for 24 h and 48 h. Apoptosis was detected by flow cytometry using an Annexin V/7-AAD staining and representative figures (including gating strategy) are shown. (B) MM cell lines were treated with tasquinimod (10, 25 μM) for 3 and 5 days. Apoptosis was analysed by Annexin V/7-AAD staining (n=4). *$p < 0.05$, **$p < 0.01$, ***$p < 0.001$, ***$p < 0.0001$, Error bars indicate SD, Ordinary one-way ANOVA.

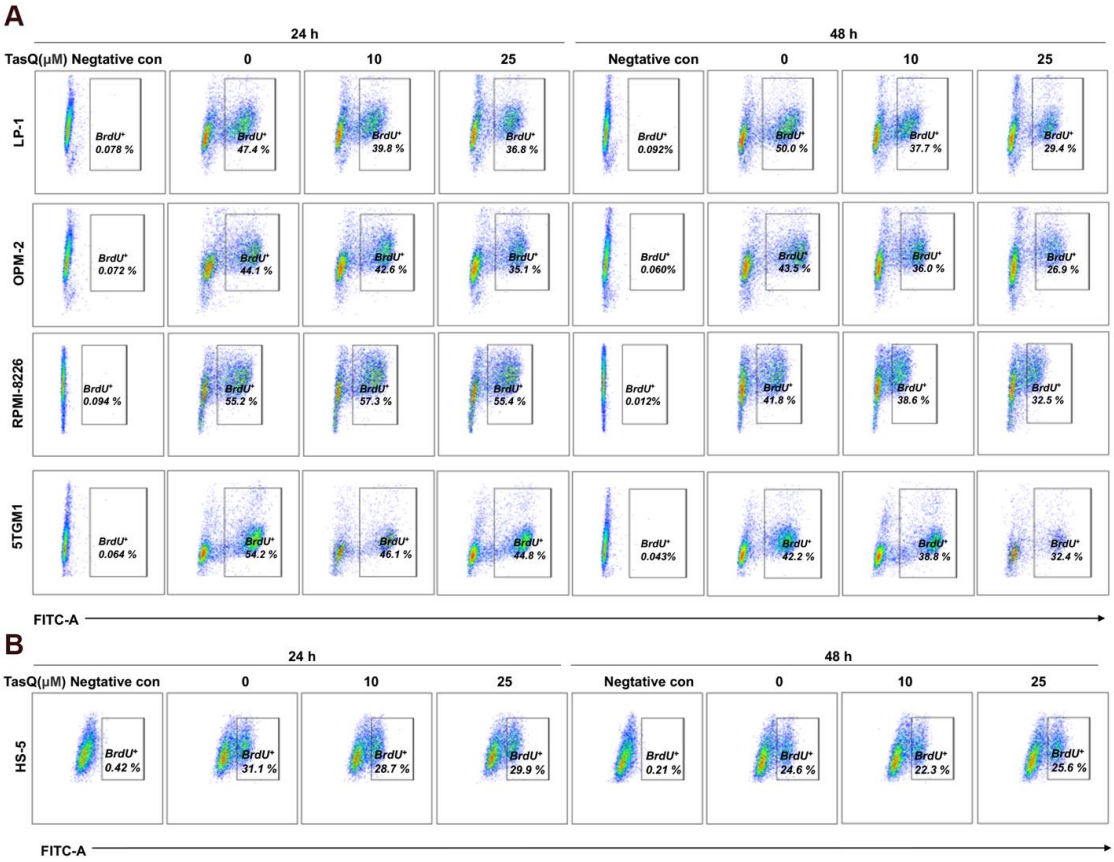

Supplemental Figure 2. Tasquinimod inhibits MM cell proliferation. MM cell lines (LP-1, OPM-2, RPMI-8226 and 5TGM1) and the stromal cell line HS-5 were treated with tasquinimod (TasQ) (10, 25 μM) for 24 h and 48 h. Cell proliferation was analyzed using BrdU staining and flow cytometry. Representative figures and the gating strategy are shown for MM cell lines (A) and HS-5 cells (B).

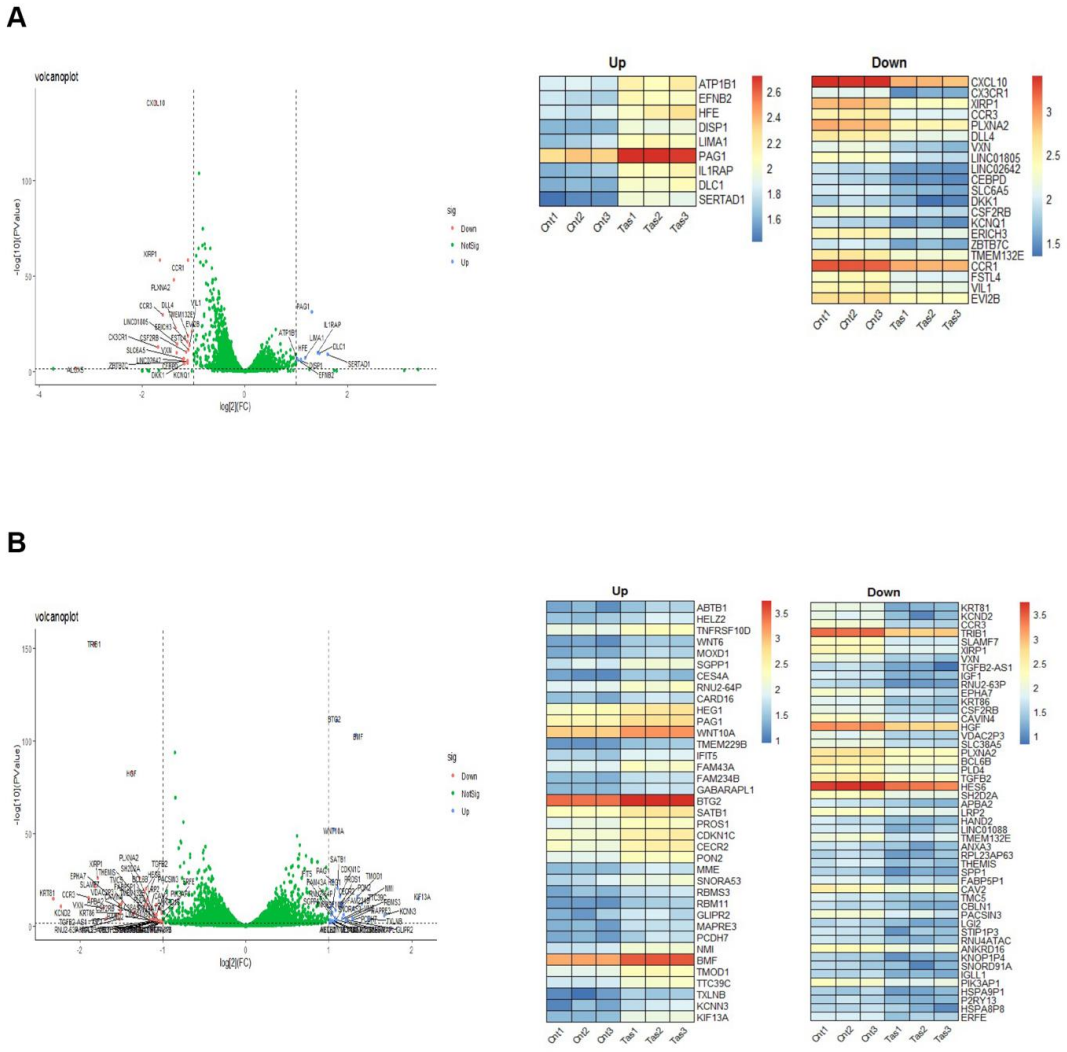

Supplemental Figure 3. Gene profile analysis in LP-1 cells after tasquinimod treatment. Volcano plot (left) comparing vehicle versus tasquinimod treatment. Heat map (right) showing differential gene expression in top-ranked genes in LP-1 cells after treatment with either 25 µM of tasquinimod (Tas) or DMSO (cnt) for 6 h (A) and 24 h (B). The experiments were done in 3 biological triplates and represented by 3 columns for each condition.

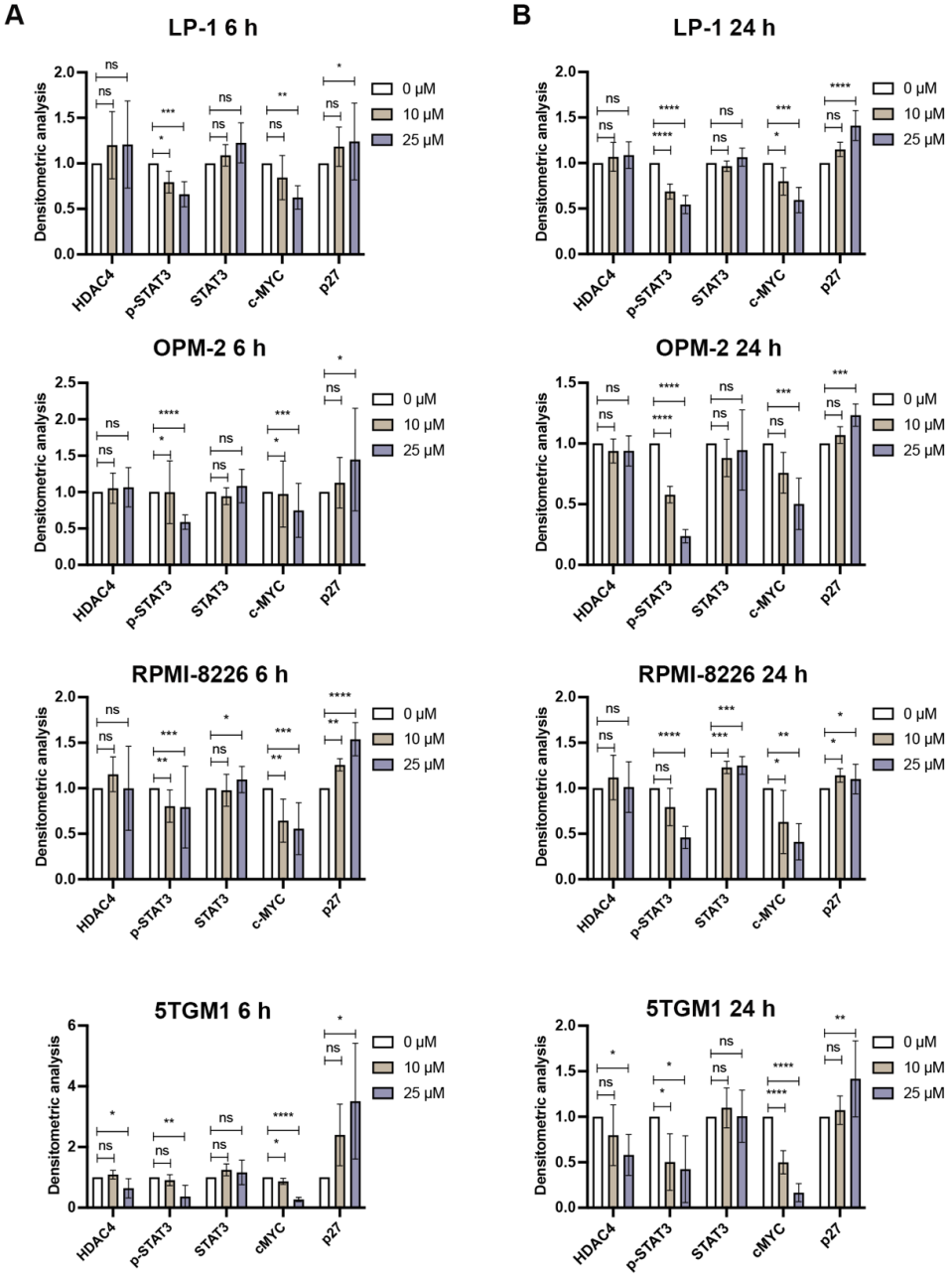

Supplemental Figure 4. Grayscale analyses of western blots in Figure 2. Human MM cell lines (LP-1, OPM-2, RPMI-8226) and the murine 5TGM1 cell line were treated with tasquinimod (10 μM, 25 μM) for 6 h (A) and 24 h (B) (n=5). Western blot signals were analyzed using ImageJ software. *p < 0.05, **p < 0.01, ***p < 0.001, ***p < 0.0001, Error bars indicate SD, Ordinary one-way ANOVA.

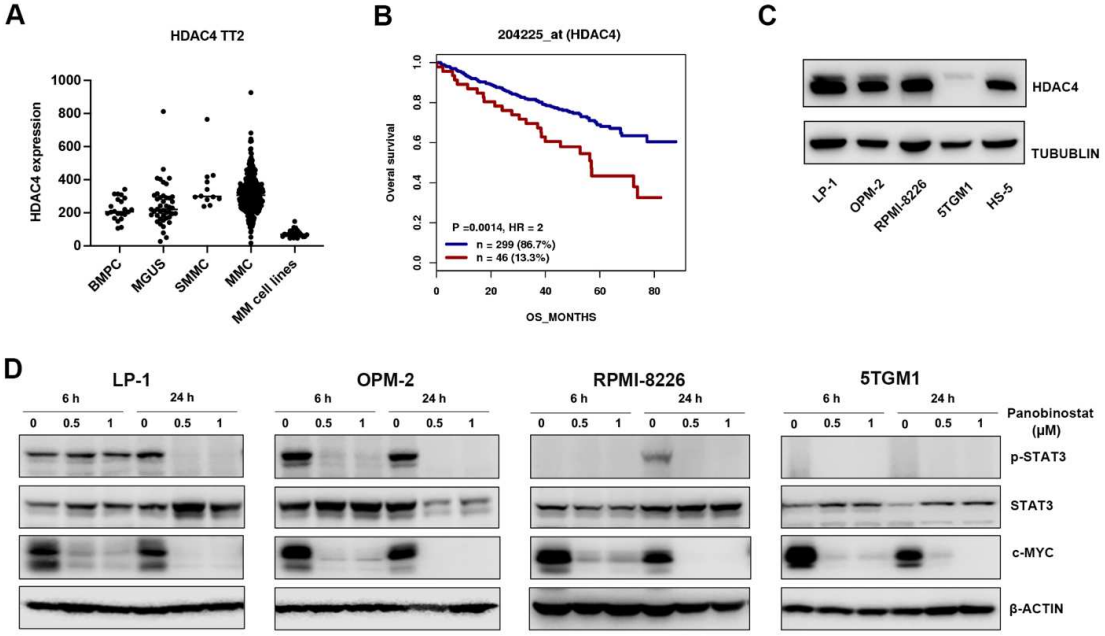

Supplemental Figure 5. HDAC4 correlates with a poor prognosis and targeting of histone deacetylases using panobinostat results in a similar decrease of c-MYC and p-STAT3. (A) The scatter plot of HDAC4 expression in BMPC (n=22), MGUS (n =44), SMMC (n=12), MMC (n=345), primary MM cell lines (n=23) samples using gene expression profiling (GEP) data using the online web tool Genomicscape. (B) Kaplan-Meier curve show the correlation of HDAC4 expression with overall survival (OS) in the TT2 MM patient cohort. High and low scores were defined as above and below the median level of expression, respectively. Log-rank test p values are indicated on the curves (p = 0.0014). (C) The HDAC4 expression in different MM cell lines and the stromal cell line HS-5 was detected by western blot (n=3). (D) LP-1, OPM-2, RPMI-8226 and 5TGM1 cells were cultured with panobinostat (0.5, 1 μM) for 6 h and 24 h. Whole-cell lysates were subjected to western blot using anti– phospho-STAT3, anti–STAT3, anti–c-MYC and anti– β-ACTIN antibodies (n=3).

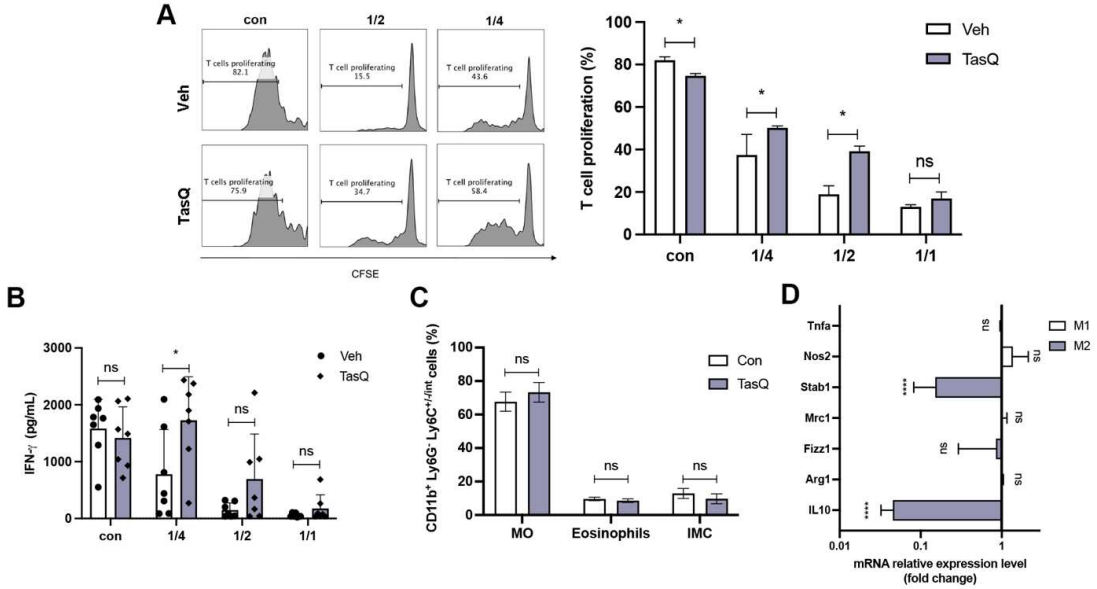

Supplemental Figure 6. Tasquinimod reduces the MDSC suppressive capacity in 5T33MM-derived conditioned medium *in vitro*. (A) MACS sorted CD11b$^+$ bone marrow cells were co-cultured in the presence of 5T33MM conditioned medium, CD3/CD28 microbeads and splenic CFSE-labeled T cells of naive mice. MDSC and T cells were co-cultured at a ratio of 1/4, 1/2 and 1/1 respectively. After 72 h, T cell proliferation was analyzed using flow cytometry (n = 3, Mann-Whitey U test). (B) Supernatant was collected from this assay and IFN-γ secretion was analyzed using ELISA (n=7, Mann-Whitey U test). (C) CD11b$^+$ cells were sorted from the bone marrow of the 5T33MM model and treated with vehicle or tasquinimod (TasQ) for 24 h. The MDSC phenotype was evaluated via flow cytometry (n=3, Mann-Whitey U test). (D) CD11b$^+$ cells were sorted from the bone marrow of the 5T33MM model and treated with vehicle or tasquinimod for 6 h. The mRNA level of genes was measured with RT-qPCR and calculated with the ΔΔC. The data are expressed relative to their respective controls set to 1 (n=4, Unpaired t-test). *$p < 0.05$; ****$p < 0.0001$, Error bars indicate SD.

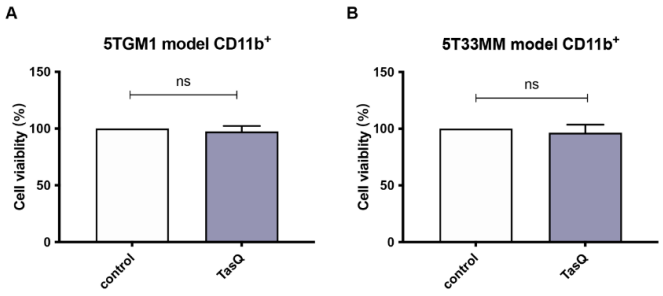

Supplemental Figure 7. Tasquinimod has no direct effect on the cell viability of MM-derived MDSC *in vitro.* MACS-sorted CD11b$^+$ cells from the 5TGM1 (A) and 5T33MM (B) model were treated with/without tasquinimod (TasQ) (25 µM) for 24 h and cell viability was analyzed (n=4). Unpaired t-test. Error bars indicate

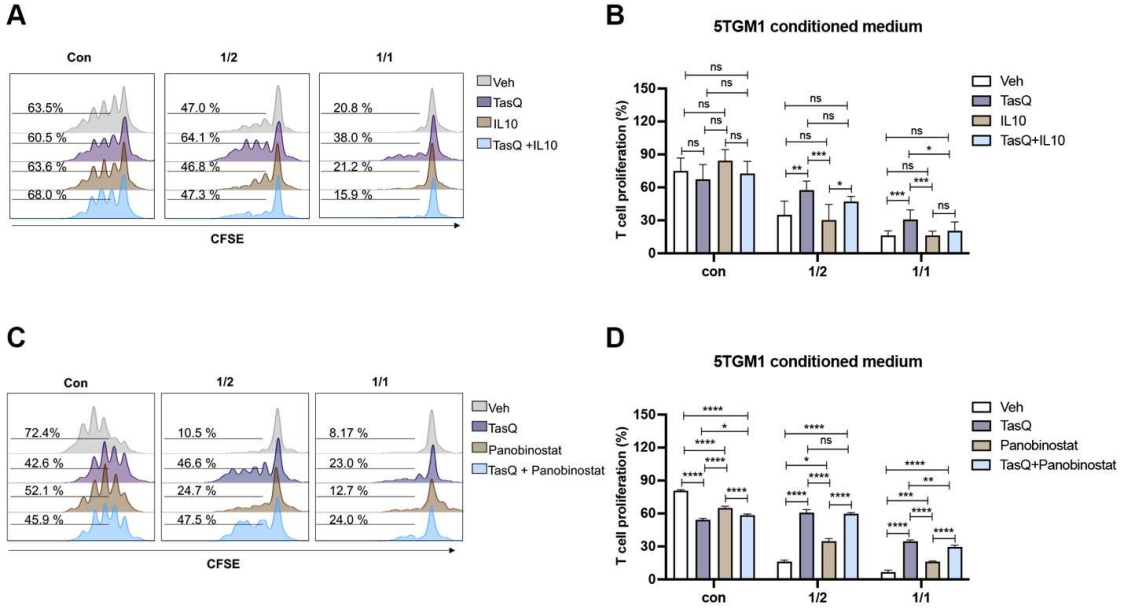

SD.

Supplemental Figure 8. **Recombinant IL-10 and panobinostat change the T cell proliferation capacity in the presence of MDSC, with/without the treatment of tasquinimod.** MACS sorted CD11b$^+$ bone marrow cells were co-cultured in the presence of 5TGM1 conditioned medium, CD3/CD28 microbeads and splenic CFSE-labeled T cells of naïve mice, with/without tasquinimod (TasQ) (25 µM). MDSC and T cells were co-cultured at a ratio of 1/2 and 1/1 respectively. (A-B) Recombinant IL-10 was added at a concentration of 100 ng/mL and T cell proliferation was analyzed after 72 h (n=6). (C-D) Panobinostat was added to the assay at a concentration

of 10 nM and T cell proliferation was analyzed after 72 h (n=3). * $p < 0.05$, ** $p < 0.01$, *** $p < 0.001$, **** $p < 0.0001$, One-way ANOVA. Error bars indicate SD.

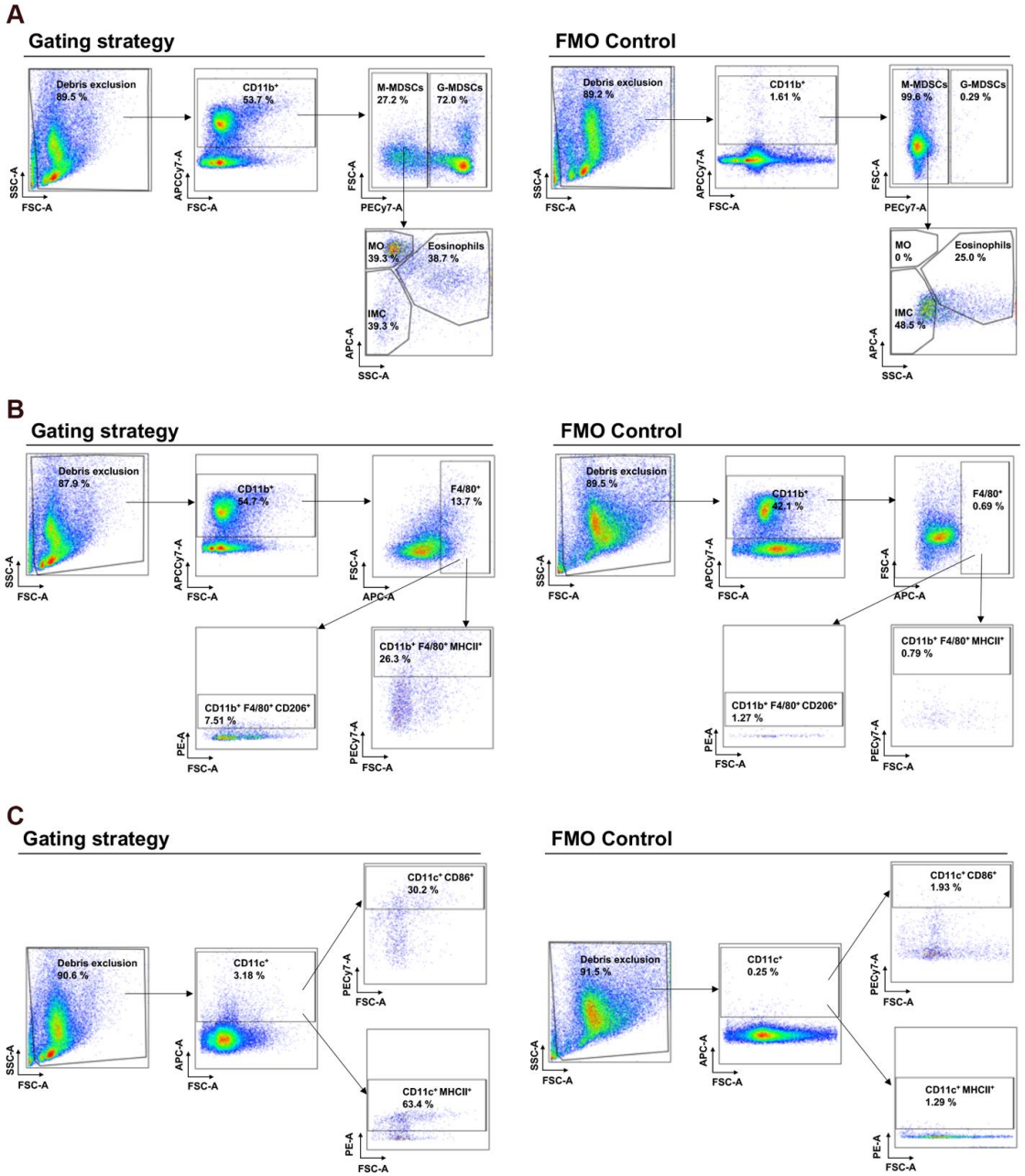

Supplemental Figure 9. The flow cytometry gating strategy and FMO controls of myeloid cell populations in the 5TGM1 model. (A) CD11b^{+} cells, M-MDSCs, G-MDSCs, Ly6C^{hi} inflammatory monocytes (MO), Ly6C ^{intermediate} eosinophils, and Ly6C^{low} immature myeloid cells (IMC). (B) Macrophages. (C) Dendritic cells.

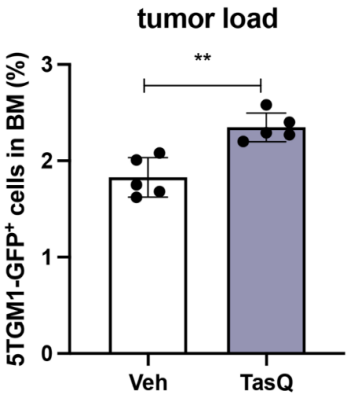

Supplemental Figure 10. The percentage eGFP positive tumor cells in the bone marrow of tasquinimod-treated 5TGM1 mice after 10 days. 6-week-old C57BL/KaLwRij mice were inoculated with 1.0 × 10^{6} 5TGM1-eGFP cells on day 0 and treatment with tasquinimod (TasQ, 30 mg/kg in daily drinking water) started on day 1 (n=5/group). At day 10, all mice were sacrificed to investigate immune cell populations using flow cytometry. $^{**}p < 0.01$, Error bars indicate SD, Mann-Whitey U test.